

Questioning Normality: A study of wavelet leaders distribution

Wejdene Ben Nasr^{1†}, Hélène Halconruy^{2,3*†}, Stéphane Jaffard^{1†}

¹*LAMA, Univ Paris Est Creteil, Univ Gustave Eiffel CNRS, Créteil, F-94010, France.

²SAMOVAR, Télécom SudParis, Évry-Courcouronnes, France.

³Modal'X, Nanterre Université, Nanterre, France.

*Corresponding author(s). E-mail(s):

helene.halconruy@telecom-sudparis.eu;

Contributing authors: wejdene.nasr-ben-hadj-amor@u-pec.fr;

jaffard@u-pec.fr;

†These authors contributed equally to this work.

Abstract

The motivation of this article is to estimate multifractality classification and model selection parameters : the first-order scaling exponent \mathbf{c}_1 and the second-order scaling exponent (or intermittency coefficient) \mathbf{c}_2 . These exponents are built on wavelet leaders, which therefore constitute fundamental tools in applied multifractal analysis. While most estimation methods, particularly Bayesian approaches, rely on the assumption of log-normality, we challenge this hypothesis by statistically testing the normality of log-leaders. Upon rejecting this common assumption, we propose instead a novel model based on log-concave distributions. We validate this new model on well-known stochastic processes, including fractional Brownian motion, the multifractal random walk, and the canonical Mandelbrot cascade, as well as on real-world marathon runner data. Furthermore, we revisit the estimation procedure for \mathbf{c}_1 , providing confidence intervals, and for \mathbf{c}_2 , applying it to fractional Brownian motions with various Hurst indices as well as to the multifractal random walk. Finally, we establish several theoretical results on the distribution of log-leaders in random wavelet series, which are consistent with our numerical findings.

Keywords: Log-concave distributions, multifractal analysis, random wavelet series, scaling exponent estimation, wavelet leaders.

1 Introduction

The motivation behind this paper is to estimate regularity parameters, namely c_1 and c_2 , which represent the first- and second-order scaling exponents. These parameters are crucial for tasks such as signal and texture classification, with applications in biomedicine, as well as for analyzing fully developed turbulence. They also play a key role in selecting suitable mathematical or stochastic models that exhibit multifractal behavior in fields such as finance, geophysics, and fluid dynamics.

A common approach involves directly estimating local regularity, often using fractional processes, including extensions of fractional Brownian motion (fBm) to capture local variations [1, 2]. Techniques based on local increments [3, 4] and wavelets [5–7] have been widely explored. However, direct estimation faces key limitations, including assumptions about process types (e.g., multifractional processes), reliance on small data intervals, and instability when dealing with multiplicative cascades or Lévy processes with erratic exponents. These challenges underscore the importance of global estimation methods, shifting the focus to multifractal analysis.

The purpose of multifractal analysis is to estimate the sizes of sets where pointwise regularity takes specific values (referred to as the *multifractal spectrum*, first defined in the seminal paper by Frisch and Parisi [8], see Section 2.1). This approach exploits scaling properties from log-log plots of empirical moments of order $p \in \mathbb{R}$, as originally proposed by Kolmogorov [9]. Initially restricted to $p > 0$ in [8], these methods were later extended to allow both positive and negative values of p , leading to methods such as WTMM (Wavelet Transform Maxima Method) [10] and DFA (Detrended Fluctuations Analysis) [11]. However, these methods lacked theoretical results linking them to the multifractal spectrum.

State-of-the-art multifractal analysis now relies on orthonormal wavelet decompositions, where multiscale quantities derived from the suprema of wavelet coefficients—known as *wavelet leaders*—are used to compute scaling functions ζ_f (see Definition 4 below). Their Legendre transforms provide an upper bound for the multifractal spectrum. These methods have proven effective in applications such as model selection and classification. For instance, the estimation of moments for negative values of p has been used to reject turbulence models whose scaling functions did not align with those measured from experimental data [10, 12]. However, reliable applications require a statistical framework that provides confidence intervals.

An important step was the introduction by Abry and Wendt of bootstrap methods to estimate scaling exponents, improving accuracy when only a few scales are available [13–15]. In practice, rather than relying on the entire scaling function, a few coefficients from its Taylor expansion at $p = 0$, computed as log-cumulants, are often sufficient. The first two cumulants, c_1 and c_2 , capture key multifractal properties: c_1 represents the most frequently observed pointwise regularity exponent, while c_2 quantifies fluctuations in local regularity. Bayesian methods introduced by Combexelle, Wendt, Dobigeon, Tourneret, McLaughlin, and Abry, under the assumption of log-normality, have significantly improved the estimation of these quantities [16–18]. The third major multifractality parameter used in classification and model selection,

the *uniform regularity exponent* H_f^{\min} , is of a different nature, as it is derived directly from wavelet coefficients rather than wavelet leaders. Its statistical estimation will be addressed in [19].

Motivated by the estimation of the scaling parameters c_1 and c_2 , we challenge the commonly assumed log-normality hypothesis, which is often used to justify Bayesian methods and bootstrap approaches. We explore key modeling and statistical questions: Is the log-normality assumption valid for widely studied stochastic processes? To what extent does it hold for real-world signals? When it fails, can more flexible statistical models better capture the observed distributions of wavelet leaders?

To address these questions and empirically validate our statistical model, we first test for normality. We show that, in general, the log-leaders associated with standard stochastic models - such as fractional Brownian motion (fBm), the canonical Mandelbrot cascade, and the multifractal random walk - as well as those derived from real-world marathon runner data, are not Gaussian. This motivates us to consider a broader non-parametric framework: *log-concave distributions*. We then apply a log-concavity test developed by Cule, Samworth, and Stewart [20] to the underlying densities, independently of whether wavelet coefficients across scales exhibit dependencies. We illustrate these findings using the same well-known stochastic models and marathon data.

Moving beyond log-normality while leveraging log-concavity and finite variance, we revisit a simple estimation method for c_1 and c_2 based on the central limit theorem, providing confidence intervals and comparing our results with standard bootstrap methods.

Although dependencies between scales are empirically evident, the literature often assumes independence [21] to facilitate calculations. Adopting this approximation, we conduct a theoretical study of the distribution of wavelet leaders in random wavelet series, which supports the log-concavity model observed numerically. This theoretical and exploratory work represents an initial step toward modeling the distribution of log-leaders, a direction to be further explored in future research.

The paper is organized as follows. In Section 2, we define log-leaders and motivate their study by positioning them within the broader context of multifractal analysis, emphasizing its key concepts and results. Section 3 introduces a new empirically validated statistical model for log-leaders: *log-concave distributions*. We first challenge the common assumption of normality for log-leaders in Section 3.1, demonstrating through both theoretical models and real-world data that this hypothesis must be rejected. We then test the hypothesis of log-concavity for their distributions in Section 3.2. Assuming log-concavity, we revisit the estimation of c_1 and c_2 using the central limit theorem and provide confidence intervals in Subsection 4. Section 5 presents a brief theoretical analysis of the distribution of log-leaders in random wavelet series, which aligns with the empirical findings from the previous section. Finally, we conclude in Section 6, offering insights and suggesting directions for future research.

2 Multifractal analysis

2.1 Pointwise regularity and multifractal spectrum

Let $x \in \mathbb{R}^d \mapsto X(x)$ denote the function or sample path of a stochastic process, or random field, in d variables. In order to examine the analytical characteristics of X , it is essential to define a pointwise regularity exponent of X at each point x . The *Hölder exponent* is the most commonly employed notion for pointwise regularity.

Definition 1 Let $X : x \in \mathbb{R}^d \mapsto X(x)$ be a locally bounded function, $x_0 \in \mathbb{R}^d$, and let $\alpha \geq 0$; X belongs to $C^\alpha(x_0)$ if there exist a constant $C > 0$, $r > 0$ and a polynomial P of degree less than α , such that

$$\text{If } |x - x_0| \leq r, \text{ then } |X(x) - P(x - x_0)| \leq C|x - x_0|^\alpha. \quad (1)$$

The Hölder exponent of X at x_0 is

$$h_X(x_0) = \sup \{ \alpha : X \in C^\alpha(x_0) \}. \quad (2)$$

Following the initial intuition of Frisch and Parisi [8], a relevant size information on the sets of singularities of X is provided by the following notion.

Definition 2 Let $X : \mathbb{R}^d \mapsto \mathbb{R}$ be a locally bounded function. The multifractal spectrum of X is the function \mathcal{D}_X defined on \mathbb{R} by

$$\forall H \in \mathbb{R}, \quad \mathcal{D}_X(H) = \dim(\{x : h_X(x) = H\}), \quad (3)$$

where \dim denotes the Hausdorff dimension (with the convention, $\dim(\emptyset) = 0$).

In applications, the purpose of multifractal analysis is to obtain numerically robust estimates of the multifractal spectrum. The state-of-the-art methods are based on the wavelet characterization of the Hölder exponent, which we review in the next section.

2.2 Wavelet based characterization of Hölder exponent

2.2.1 Orthonormal wavelet bases

Let $\{\psi^{(i)}\}_{i=1, \dots, 2^d-1}$ be a set of *mother wavelets*, each of them being a smooth function with fast decay such that the $\psi^{(i)}$ and their derivatives up to a given order N_ψ have fast decay. Furthermore, the set of dilated (to scales 2^j) and translated (to space/time location $2^j k$) templates

$$\{2^{dj/2} \psi^{(i)}(2^{-j}x - k)\} \quad \text{for } i = 1, \dots, 2^d - 1, j \in \mathbb{Z}, k \in \mathbb{Z}^d, \quad (4)$$

forms an orthonormal basis of $L^2(\mathbb{R}^d)$, see [22, 23]. This implies that the mother wavelets $\{\psi^{(i)}\}_{i=1, \dots, 2^d-1}$ possess vanishing moments: $\int_{\mathbb{R}} P(x) \psi^{(i)}(x) dx = 0$ for any polynomial P of degree strictly smaller than N_ψ . The *wavelet coefficients* of a function X are defined for $i = 1, \dots, 2^d - 1, j \in \mathbb{Z}, k \in \mathbb{Z}^d$ as

$$c_{j,k}^{(i)} = 2^{dj} \int_{\mathbb{R}^d} X(x) \psi^{(i)}(2^{-j}x - k) dx, \quad (5)$$

where an L^1 normalization is used for wavelet coefficients.

2.2.2 Wavelet leaders

Wavelet leaders are multiscale quantities that provide significant advantages over traditional wavelet coefficients in multifractal analysis, both theoretically and practically [24, 25]. These properties make them particularly well-suited for developing a multifractal formalism, as will be discussed in Section 2.3.

Definition 3 Let X be a locally bounded function. The wavelet leaders of X are defined as

$$\ell_{j,k} = \ell_\lambda = \sup_{\lambda' \subset 3\lambda} |c_{\lambda'}|, \quad (6)$$

where $k = (k_1, \dots, k_d)$, $\lambda = \lambda_{j,k} = [k_1 2^{-j}, (k_1 + 1) 2^{-j}) \times \dots \times [k_d 2^{-j}, (k_d + 1) 2^{-j})$ denotes the dyadic cube of scale j , 3λ denotes the homothetic cube with same center and three times wider, and λ' is a dyadic cube included in 3λ (λ' has width $2^{-j'}$ with $j' \geq j$).

A key property of wavelet leaders is that, under a mild uniform regularity assumption on X , they allow to recover the Hölder exponent in the limit of fine scales through a log-log plot regression, see [24].

Proposition 1 Let $X : \mathbb{R}^d \rightarrow \mathbb{R}$ be such that

$$\exists \varepsilon > 0 : \quad X \in C^\varepsilon(\mathbb{R}^d). \quad (7)$$

Then, the Hölder exponent of X at x_0 can be recovered from the wavelet leaders of X by

$$h_X(x_0) = \liminf_{j \rightarrow +\infty} \frac{\log(\ell_{\lambda_{j,k}}(x_0))}{\log(2^{-j})}, \quad (8)$$

where $\lambda_{j,k}(x_0)$ the unique dyadic cube of length 2^{-j} which includes x_0 .

When the relationship (8) holds between a nonnegative quantity $d_{j,k}$ and a pointwise exponent h , one says that the $d_{j,k}$ form a *multiresolution quantity associated with the exponent h* .

2.3 Multifractal formalism based on wavelet leaders

In practical applications, multifractal analysis provides a global approach to characterizing the fluctuations of h_X across time or space, as captured by the multifractal spectrum. This spectrum can be estimated from data using the mathematical frameworks known as *multifractal formalisms*. In this article, we focus on the specific formalism adapted to pointwise Hölder regularity, which is based on *wavelet leaders*; see [26].

Definition 4 Let $X \in L^\infty_{\text{loc}}(\mathbb{R}^d)$, the leader structure functions are defined as the sample moments of the wavelet leaders

$$\forall q \in \mathbb{R}, \quad S_\ell(j, q) = 2^{-dj} \sum_k |\ell_{j,k}|^q. \quad (9)$$

The leader scaling function of X is

$$\forall q \in \mathbb{R}, \quad \zeta_X(q) = \liminf_{j \rightarrow +\infty} \frac{\log(S_\ell(j, q))}{\log(2^{-j})}. \quad (10)$$

Note that (10) implies that, in the limit of fine scales, $S_\ell(j, q)$ exhibits a power law behavior with respect to the scale 2^{-j} , $S_\ell(j, q) \approx F_q 2^{-j\zeta_X(q)}$. The function $\zeta_X(q)$ is necessarily concave, see [26]; the multifractal formalism is defined via the Legendre transform of the mapping $q \mapsto \zeta_X(q)$.

Definition 5 The leader Legendre spectrum is defined by

$$\forall H \in \mathbb{R}, \quad \mathcal{L}_X(H) = \inf_{q \in \mathbb{R}} (d + qH - \zeta_X(q)). \quad (11)$$

If (7) holds, then \mathcal{L}_X provides an upper bound of the multifractal spectrum of X (see [27]):

$$\forall H \in \mathbb{R}, \quad \mathcal{D}_X(H) \leq \mathcal{L}_X(H). \quad (12)$$

This result follows from (8): it holds because wavelet leaders $\ell_{j,k}$ are multiresolution quantities associated with the exponent h_X . Consequently, from a mathematical perspective, the Legendre spectrum based on wavelet leaders provides information about the sizes of singularity sets in the data that would not be accessible if one were to use wavelet coefficients directly (i.e., if the *wavelet scaling function* were employed instead).

From a numerical standpoint, using wavelet coefficients for $q < 0$ in the definition of the structure function leads to numerical instabilities for the following reason. If X is a random variable, consider its corresponding probability distribution function (PDF):

$$\text{for } A \geq 0, \quad F_X(A) = \mathbb{P}(|X| \leq A). \quad (13)$$

For many models and in a wide range of applications, the function F_X associated with wavelet coefficients at a given scale is of the form

$$F_X(A) \sim c + c' A \quad (14)$$

(after appropriate rescaling). This is the case, for example, in the widely used generalized Gaussian mixture models; see [19, 28, 29]. The case $c \neq 0$ corresponds to mixtures that include a Dirac mass at the origin, meaning that X has no moments of negative order. A linear behavior of $F_X(A)$ for small A is observed, for instance, in distributions with continuous and nonvanishing densities for small A ; in this case, X has moments of order $q > -1$. Additionally, for wavelet coefficients, the empirical moments

$$2^{-j} \sum_{i,k} |c_{j,k}^{(i)}|^q$$

which are estimated are numerically highly unstable and are not shift invariant (an appropriate shift of the data can make a wavelet coefficient vanish). However, these

moments yield no relevant information on the pointwise regularity of the sample paths because they do not include information on the correlations of the locations of small wavelet coefficients which is crucial for inferring the existence of large values taken by the Hölder exponent (see e.g. [25] where the example of the sample paths of Brownian motion is studied, showing that the Legendre spectrum based on wavelet coefficients does not yield the multifractal spectrum because of the values taken by negative moments). In [19] a detailed exposition of these questions will be given together with its implications for the multifractal analysis of the sample paths of the corresponding processes.

The poor behavior of scaling functions based on wavelet coefficients for $q < 0$ contrasts sharply with those based on wavelet leaders. Small values of wavelet leaders indicate that nearby wavelet coefficients also take small values, an event much less likely if the coefficients are independent or weakly correlated. This highlights the ability of wavelet leaders to capture correlations between the locations of small wavelet coefficients.

For many signal classes, the PDF (13) of wavelet leaders is extremely small for small A , resulting in distributions with finite moments of all orders. See [30] for a discussion on how shuffling wavelet coefficients at each scale affects wavelet leader statistics, and [31] for numerical evidence of significant discrepancies between the statistics of wavelet coefficients and wavelet leaders for small A .

These theoretical and practical considerations justify the use of both positive and negative values in the structure functions (9) as a valuable classification tool. This motivates the study of log-leader distributions in Section 3 and their relevance for estimating multifractality parameters in Section 4.

Returning to our initial motivation, we now recall how classification parameters are derived from log-leaders. A key observation is that the leader structure functions $S_\ell(j, q)$, defined in (9), can be interpreted as sample mean estimators for the ensemble averages $\mathbb{E}[|\ell_{j,k}|^q]$ (assuming these quantities are finite). According to (10), they exhibit a power-law behavior in the limit of small scales, so that

$$\mathbb{E}[|\ell_{j,k}|^q] \approx S_\ell(j, q) \approx F_q 2^{-j\zeta_X(q)}, \quad j \rightarrow +\infty. \quad (15)$$

Building on the heuristic analysis introduced in [32] with increments as multiresolution quantities, and later refined for continuous wavelet coefficients in [33], we recall the extended interpretation that includes wavelet leaders, see [14, 34–36] and references therein. Assume that (15) holds on a small interval around $q = 0$; taking the logarithm of both sides of (15) yields the standard cumulant-generating function expansion

$$\log[\mathbb{E}(e^{q \log(|\ell_{j,k}|)})] = \log(\mathbb{E}[|\ell_{j,k}|^q]) = \log(F_q) + \zeta_X(q) \log(2^{-j}) = \sum_{m \geq 1} C_m(j) \frac{q^m}{m!}, \quad (16)$$

where $C_m(j)$ denotes the m -th order cumulant of the random variables $\log(|\ell_{j,k}|)$. From (16), the cumulants $C_m(j)$ must be of the form

$$C_m(j) = c_{0,m} + c_m \log(2^{-j}). \quad (17)$$

Combining (16) and (17) gives

$$\log(F_q) + \zeta_X(q) \log(2^{-j}) = \sum_{m \geq 1} c_{0,m} \frac{q^m}{m!} + \sum_{m \geq 1} c_m \frac{q^m}{m!} \log(2^{-j}). \quad (18)$$

Thus, $\zeta_X(q)$ can be expanded around $q = 0$ as

$$\zeta_X(q) = \sum_{m \geq 1} c_m \frac{q^m}{m!}. \quad (19)$$

Equation (17) provides a direct method to estimate the coefficients c_m , known as log-cumulants, via linear regressions of $C_m(j)$ against $\log(2^{-j})$. Furthermore, assuming $c_2 \neq 0$, the polynomial expansion (19) can be transformed into an expansion of \mathcal{L}_X around its maximum using the Legendre transform (11), see [15, 25, 34]

$$\mathcal{L}_X(H) = d + \frac{c_2}{2!} \left(\frac{H - c_1}{c_2} \right)^2 + \text{remainder}. \quad (20)$$

Estimating the multifractal spectrum of X entails the theoretical task of evaluating $\zeta_X(p)$ across a broad range of p values and computing its Legendre transform. Equation (20) provides an alternative approach based on estimating a few parameters c_p , which offer a concise synthesis of the multifractal characteristics of the signal X . The first log-cumulant c_1 , for example, indicates the location of the maximum of the multifractal spectrum \mathcal{D}_X and can be interpreted as the almost-everywhere regularity of X . Meanwhile, the coefficient c_2 , often referred to as the *multifractality parameter*, quantifies the width of \mathcal{D}_X , reflecting the range of values taken by the Hölder exponent of the signal. However, it is important to note that the expansion in (19) is not universally valid. Specifically, it requires that the derivatives of ζ_X exist in a neighborhood of $q = 0$, a condition that is not satisfied by all processes. Consequently, this article focuses on processes for which (19) remains valid up to the first few orders. Since estimating the Legendre transform \mathcal{L}_X relies on the log-cumulants of the log-leaders, understanding their distribution becomes essential. This is the focus of the next two sections. Estimating the multifractal spectrum of X entails the theoretical task of evaluating $\zeta_X(p)$ across a broad range of p values and computing its Legendre transform. Equation (20) provides an alternative approach based on estimating a few parameters c_p , which offer a concise synthesis of the multifractal characteristics of the signal X .

The first log-cumulant c_1 , for example, indicates the location of the maximum of the multifractal spectrum \mathcal{D}_X and can be interpreted as the almost-everywhere regularity of X . Meanwhile, the coefficient c_2 , often referred to as the *multifractality parameter*, quantifies the width of \mathcal{D}_X , reflecting the range of values taken by the Hölder exponent of the signal. However, it is important to note that the expansion in (19) is not universally valid. Specifically, it requires that the derivatives of ζ_X exist in a neighborhood of $q = 0$, a condition that is not satisfied by all processes. Consequently, this article focuses on processes for which (19) remains valid up to the first few orders.

Since estimating the Legendre transform \mathcal{L}_X relies on the log-cumulants of the log-leaders, understanding their distribution becomes essential. This is the focus of the next two sections.

3 Statistical model of log-leaders

As detailed earlier, a key component of multifractal analysis is estimating the multifractal spectrum, which describes the distribution of singularities across scales, achieved numerically by computing wavelet leaders. In this section, we focus on their distribution through the following two questions:

[1] Questioning the normality of log-leaders Previous works have often assumed that log-leaders follow a Gaussian distribution [16, 17, 34, 37, 38], based on analyses using QQ-plots, which graphically compare the quantiles of two distributions (see Section 3.1.1). These plots suggest a visual agreement between the empirical quantiles of log-leaders and those of a standard normal distribution. However, this method has only been experimentally applied to certain self-similar processes and multifractal multiplicative cascades [37], leaving the normality assumption unverified for other stochastic processes and possibly unreliable for real-world data. In Subsection 3.1, we aim to test this assumption in different contexts, showing that despite a good visual fit, classical normality tests do not support this assumption for many theoretical and real-world data sets.

[2] A new model for the law of log-leaders: log-concave distributions Our second aim is to present a more general methodology by moving beyond the restrictive normality assumption and focusing, in Section 3.2, on a more flexible hypothesis: log-concavity of the underlying distributions. Log-concavity is a powerful statistical assumption that encompasses normality while applying to a broader range of distributions. This added flexibility allows to model the complexity of multifractal data without imposing excessive constraints. Our methodology involves using a statistical procedure to test whether log-leader distributions are log-concave, without assuming a specific form. This approach provides a more robust characterization of the underlying structures in the studied signals. It represents a significant advancement by moving beyond the limiting assumption of normality, thereby paving the way for more nuanced analyses suitable for the diverse behaviors observed in fields such as finance, biology, and other applications where multifractality prevails.

3.1 Checking the normality assumption of log-leaders

As mentioned in the introduction, it is commonly assumed in the multifractal analysis literature that log-leaders are normally distributed (e.g. [16, 17, 34, 37, 38]). The objective of this section is to challenge this hypothesis by applying a normality test to the log-leaders calculated from simulated processes (fractional Brownian motion, compound Poisson motion...) and real physiological data from marathon runners. Most of the numerical results are obtained using a Daubechies mother wavelet ψ with $N_\psi = 3$ vanishing moments. At the end of Subsection 3.2.5, to discuss the robustness of our results with respect to a change of wavelet basis, we compare them in the specific

case of a multifractal random walk using two different Daubechies mother wavelets, ψ , with $N_\psi = 1$ and $N_\psi = 4$.

3.1.1 Graphical method: Quantile-quantile plots

The normal quantile-quantile plot (Q-Q plot) is the most commonly used and effective diagnostic tool for checking the normality of data. It enables a graphical evaluation of the conformity between two distributions by plotting their quantiles against each other. Figure 2 illustrates Q-Q plots depicting the quantiles of the empirical distributions of log-leaders at different scales $j = 4, 5, 6$ associated with various processes and real signals, against the quantiles of the standard normal distribution. Below is a concise overview and a representative selection of the processes and real data that will be used for conducting the tests.

1. **Fractional Brownian motion (fBm):** It is the only Gaussian self-similar process with stationary increments and its multifractal properties are controlled by one single parameter, the *Hurst exponent* H , which takes values in $(0, 1)$, see [39]. For the tests we set $H = 0.4$ and $H = 0.7$.
2. **Canonical Mandelbrot Cascade motion (CMC-motion):** It is defined as $A_r(t) = \lim_{r \rightarrow 0} \int_0^t \mathcal{Q}_r(s) ds$, where \mathcal{Q}_r is the canonical Mandelbrot cascade (CMC) that represents a archetype of multifractal measure, see [40]. It is defined at resolution $r = 2^{-J}$ (i.e., after J iterations) as: $\mathcal{Q}_r(t) = c \prod_{(j,k) \in \mathcal{J}} W_{jk}$, where

$$\mathcal{J} = \{(j, k), j = 1, \dots, J \text{ and } k \text{ such that } t \in [2^{-j}k, 2^{-j}(k+1)]\},$$

the W_{jk} are the multipliers for the j -th iteration and $k = 1, \dots, 2^j$. The multipliers have to be strictly positive random variables, and satisfy the constraint $\mathbb{E}[W] = 1$, ensuring that the cascade conserves mass in average. In this work, we will only consider CMC with log-Normal multipliers $W = 2^{-U}$, where $U \sim \mathcal{N}(\mu, \sigma^2)$ is a random variable following a Gaussian distribution of mean μ and variance σ^2 . Conservation of mass implies $\sigma^2 = 2\mu/\ln(2)$, see [34]. For the numerical simulation, we use $\mu = 0.37$.

3. **Compound Poisson motion (CPM):** It is defined as $A_r(t) = \lim_{r \rightarrow 0} \int_0^t \mathcal{Q}_r(s) ds$, where \mathcal{Q}_r is the compound Poisson cascade (CPC), which is a multifractal measure based on multiplicative constructions, see [41]. The CPC signal is defined as: $\mathcal{Q}_r(t) = c \prod_{(t_i, r_i) \in C_t(t)} W_i$, where (t_i, r_i) are the positions of a two-dimensional

Poisson point process with intensity measure $dm(t, r)$ supported on the rectangle $I = \{(t, r) : r_{\min} \leq r \leq 1, -1/2 \leq t \leq T + 1/2\}$, with $r_{\min} \in (0, 1]$ and $T > 0$ being fixed; the multipliers W_i are defined below. We define the cone of influence at point t as $C_r(t) = \{(t', r') : r \leq r' \leq 1, t - r'/2 \leq t' \leq t + r'/2\}$. The normalizing constant c is defined such that $\mathbb{E}[\mathcal{Q}_r(t)] = 1$. For more details, see [42–45]. We use here CPCs with two different types of multipliers W_i :

- First, the compound Poisson cascades with log-normal (CPC-LN) multipliers of the form $W = \exp(Y)$, where $Y \sim \mathcal{N}(\mu, \sigma^2)$.
- Second, the compound Poisson cascades with log-Poisson (CPC-LP) multipliers where the multipliers W are reduced to a constant w .

The full algorithmic statement of the construction procedure of CPC's signals can be found in [46] and a visual representation is shown in [34]. Results are obtained using $T = 100$, $r_{\min} = 0.02$, $\sigma^2 = 0.2$, $\mu = -\sigma^2/2$ and $w = 3/2$.

4. **Multifractal random walk (MRW):** It stands as another notable member within the category of multifractal multiplicative cascade based processes. MRW is a non Gaussian process with stationary increments, which is defined as $X(t) = \sum_t G_H(t) \exp(W(t))$ where the $G_H(t)$ are the increments of a fractional Brownian motion with Hurst parameter H and W is a Gaussian process which is independent of G_H and with covariance $\text{cov}[(W(t_1), W(t_2))] = \beta^2 \log\left(\frac{L}{\|t_1 - t_2\| + 1}\right)$. For more details, see [47, 48]. In application we set $H = 0.6$, $N = L = 10^5$ and $\beta = 0.05$.
5. **Real data:** We use two types of physiological data from 20 amateur marathon runners: heart rate (measured in beats per minute) and speed (in m/s) of sample size ranging between 11000 and 12000 samples. These data were collected between 2023 and 2024 from different 42 km marathons using the Garmin Forerunner 630 watch and were graciously provided by V. Billat and her team. Examples of these two types of data from a marathon runner are shown in Fig. 1. We picked this particular real-life example because it is a typical case where multifractal analysis techniques have proved relevant in order to supply new insight on the physiological mechanisms that produced these data, see the articles of V. Billat and her collaborators [49–51]. For multifractal analysis, we made two choices based on the nature of the data. In the case of cardiac data, the scales were selected between $j = 5$ and $j = 7$ (i.e., between 26 s and 3 min 25 s), as they have been identified as relevant for such physiological signals [52]. Conversely, no universally recognized a priori scales exist for speed data. To address this, we determined common scales across the datasets that provided the best log-log regressions, ultimately selecting a range between $j = 5$ and $j = 8$ (i.e., between 32 s and 4 min 27 s).

These QQ-plots suggest that the normal distribution offers a reasonable approximation for the marginal distribution of log-leaders of these processes and these example of real data; this contrasts sharply with leaders, as their marginal distributions are found to significantly deviate from Gaussian distributions. Although the approximation may seem appealing, normality is a rather strong assumption, and it is therefore important to complement graphical methods with formal numerical techniques and statistical normality tests in order to robustly assess or dismiss. The formal methods which will be tried in the following section offer a more rigorous and quantitative evaluation of whether the data follow a normal distribution.

3.1.2 Numerical method: Shapiro-Wilk test

Testing normality The most common normality test procedures available in statistical toolbox are the Shapiro-Wilk test, Kolmogorov-Smirnov test, Anderson-Darling

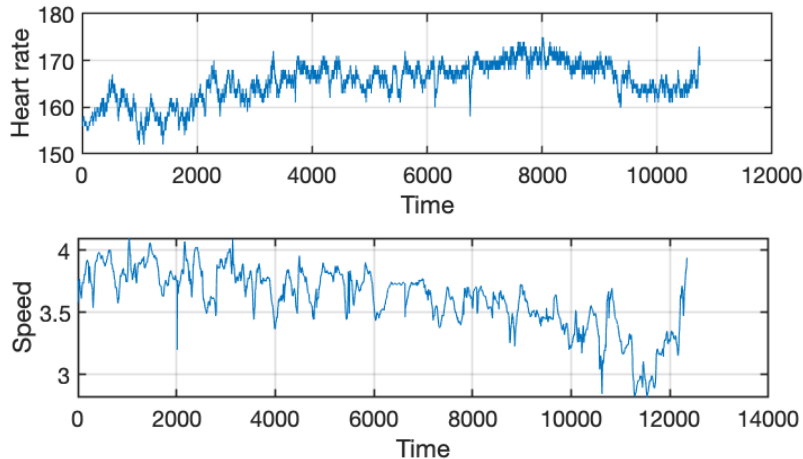


Fig. 1 Representation of two physiological data heart rate (beats per minute) and speed (kilometer per hour) of a marathon runner respectively of sample size 11000 and 12000.

test and Lilliefors test. Studies by Pala (2003) [53], Keskin (2006) [54], and Razali (2011) [55] have shown that the Shapiro-Wilk test is the most powerful normality test. It was the first test able of detecting deviations from normality caused by skewness, kurtosis, or both. Initially limited to sample sizes between 3 and 50, improvements to its algorithm have extended its applicability to data sets of up to 5000 observations (see [56–59]). The null hypothesis of this test is that the population is normally distributed, whereas the alternative hypothesis is that it is not. Thus, if the p -value is less than the chosen significance α -level, then the null hypothesis is rejected and there is evidence that the data tested are not normally distributed. On the other hand, if the p -value is greater than the chosen α -level, then the null hypothesis, i.e. the data came from a normally distributed population, cannot be rejected.

Experiments We run 1,000 simulations of various processes in MATLAB, as described above. For each simulation, we test the normality of the log-leaders $\log(\ell_{j,k})$, where $j = 4, 5, 6$ using the Shapiro-Wilk test, as detailed in Subsection 3.1.2. For each process, we report in Table 1 the proportion of times that the null hypothesis was rejected with $\alpha = 0.05$. In addition, we use physiological data (heart rate and speed) from 20 marathon runners such that for each signal we perform a normality test on log-leaders and subsequently we report in Table 2 the proportion of times where the null hypothesis was rejected. Tables 1 and 2 clearly demonstrate a significant proportion of rejections of the normality hypothesis. We observe that as j decreases, the proportion of rejections increases, indicating a stronger rejection of the normality of the log-leaders. This phenomenon can be explained by the toolbox we utilize to perform multifractal analysis and obtain the log-leaders: as j decreases, we analyze smaller scales, resulting in larger size of log-leader vector at scale j . Consequently, the statistical test becomes more precise, yielding more significant results.

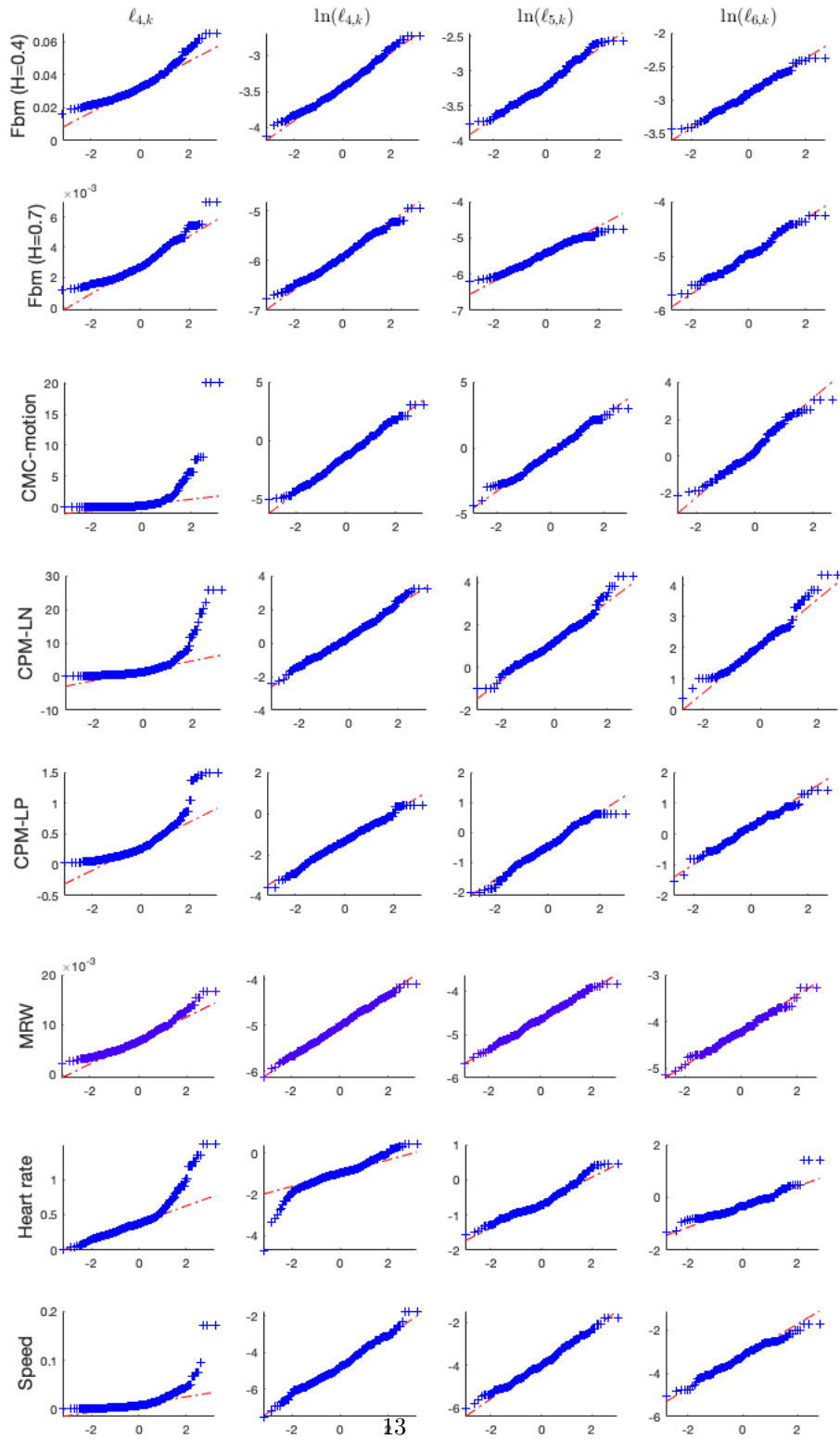


Fig. 2 Quantile-quantile plots of the empirical distributions (+) of leaders $\ell_{j,k}$ and the log-leaders $\log(\ell_{j,k})$ at several scales $j = 4, 5, 6$ against standard normal distribution (-.-) for a selection of processes of a sample size equal to 10^5 , uniformly sampled over the time interval $[0, 1]$ described in section 3.1.1; from top to bottom: fBm of Hurst exponents 0.4 and 0.7, Canonical Mandelbrot Cascade motion, two types of compound Poisson motions, multifractal random walk and finally, heart rate and speed data respectively of sample size around 11000 and 12000 collected on marathon runner.

Table 1 Empirical rejection probabilities of the Shapiro-Wilk test (see Subsection 3.1.2) applied to the log-leaders $\log(\ell_{j,k})$, $j = 4, 5, 6$ of 1000 simulations of different known processes.

X		$\log(\ell_{4,k})$	$\log(\ell_{5,k})$	$\log(\ell_{6,k})$
fBm	$H = 0.4$	0.953	0.968	0.816
	$H = 0.7$	0.842	0.681	0.624
CMC-motion		0.783	0.723	0.636
CPM-LN		0.867	0.817	0.793
CPM-LP		0.990	0.942	0.767
MRW		0.8670	0.6980	0.6250

Table 2 Empirical rejection probabilities of the Shapiro-Wilk test (see Subsection 3.1.2) applied to the log-leaders $\log(\ell_{j,k})$, $j = 4, 5, 6$ of physiological data (heart rate and speed) from 20 marathon runners.

X		$\log(\ell_{4,k})$	$\log(\ell_{5,k})$	$\log(\ell_{6,k})$
Heart rate	1	1	0.75	
Speed	1	1	0.9	

3.2 Assessing the log-concavity of log-leaders

As empirically demonstrated in the previous section, the restrictive assumption of normality for log-leaders is frequently contradicted by standard normality tests, whether applied to synthetic samples from classical mono- and multi-fractal processes or to real-life data. In this section, we introduce a non-parametric model for the density of log-leaders by considering log-concave densities. One motivation for this checking the relevance of this broader framework is that it is nonetheless relevant to carry out statistical methods in order to obtain confidence intervals, see Section 4 where these methods are mentioned.

3.2.1 Log-concave densities

The class of log-densities gathers densities on \mathbb{R}^d which are log-concave according to the following definition.

Definition 6 A function $f : \mathbb{R}^d \rightarrow [0, \infty)$ is *log-concave* if $\log(f)$ is concave, with the convention that $\log 0 = -\infty$.

Denote by \mathcal{F}_0 the set of upper-continuous log-concave densities on \mathbb{R}^d . This expansive class includes many commonly encountered parametric families. Examples of univariate log-concave densities include Gaussian densities, Gumbel densities, logistic

densities, $\Gamma(\alpha, \lambda)$ densities with $\alpha \geq 1$, $\text{Beta}(a, b)$ densities with $a, b \geq 1$ and Laplace densities. Multivariate Gaussian densities are also log-concave, as are uniform densities on convex, compact sets. Moreover, this class possesses several closure and stability properties, making it a very natural infinite-dimensional generalization of the class of Gaussian densities. Among its remarkable properties, let us mention that \mathcal{F}_0 is closed under linear transformations, marginalisation, conditioning and convolution [60, 61].

Applications Log-concave densities naturally arise in various applications, making them highly relevant for modeling. In practice, assuming that the sample distribution is log-concave rather than normal can offer significant advantages. For example, in finance, stock returns often exhibit heavy tails and asymmetry that are inadequately captured by a normal distribution (see [62]). Cryptocurrencies, with their high volatility, display even more pronounced heavy-tail returns, which are better modeled by distributions derived from the generalized gamma distribution [63]. Other applications in finance, insurance, and operations research are explored in [64] and [65]. In image processing, denoising methods assuming Gaussian noise may fail to accurately model real-world scenarios involving impulse noise; log-concave distributions like the exponential distribution better capture outliers and sudden pixel value changes [66]. Additionally, log-concave distributions simplify analysis in reliability [67] and survival theory [68], where the cumulative distribution functions (CDFs) often lack closed forms. The log-concavity of a density function implies that of its CDF, which aids statistical analysis in nonparametric frameworks [68].

Estimation and testing for log-concave densities Despite their widespread use in diverse statistical applications due to their adaptability and computational convenience, estimating log-concave densities in high-dimensional spaces presents significant challenges. Cule, Samworth, and Stewart [20] introduced an innovative method for estimating multidimensional log-concave densities using maximum likelihood estimation (MLE). They proved the existence and uniqueness of the log-concave MLE (MLE-LC) estimator \hat{f}_n and described an algorithm for its computation, which is implemented in the R package LogConcDEAD. The theoretical properties of the MLE-LC estimator were further explored in a companion paper by Cule and Samworth [69].

In the next subsection, we recall the definition of the log-concave maximum likelihood estimator introduced in [20], and describe the log-concavity test that follows. We apply this test to different processes and real-world datasets to examine the log-concavity of the associated log-leaders.

3.2.2 Log-Concave Maximum Likelihood Estimator (MLE-LC)

Let X_1, \dots, X_n be independent and identically distributed (i.i.d.) random variables with density f_0 on \mathbb{R}^d that we want to estimate, with $n \geq d + 1$. The non-parametric MLE, denoted as $\hat{f}_n^{\text{MLE-LC}}$, is defined as

$$\hat{f}_n = \hat{f}_n^{\text{MLE-LC}} := \underset{f \in \mathcal{F}_0}{\operatorname{argmax}} \prod_{i=1}^n f(X_i) = \underset{f \in \mathcal{F}_0}{\operatorname{argmax}} \log \left(\prod_{i=1}^n f(X_i) \right) \quad (21)$$

where, as a reminder, \mathcal{F}_0 denotes the class of log-concave densities on \mathbb{R}^d .

Figure 3 presents three examples of $\log(\widehat{f}_n)$ computed from the random variables $\log(\ell_{4,k})$ derived from two physiological data heart rate and speed, as well as the multifractal random walk process (MRW). It can be clearly observed that the maximum likelihood estimator \widehat{f}_n is indeed log-concave. The statistical properties of the estimator are studied in Cule and Samworth (2010) [69]. Importantly, their key finding does not rely on the assumption that the underlying density f_0 is log-concave. This is particularly noteworthy since determining the log-concavity of f_0 from a data sample is practically impossible. Thus, it becomes imperative to ensure that the estimator behaves reasonably even when this condition is not met.

We first recall that the Kullback-Leibler divergence of a density f from f_0 is given by

$$d_{\text{KL}}(f_0, f) = \int_{\mathbb{R}^d} f_0 \log\left(\frac{f_0}{f}\right) d\mu,$$

where μ is the Lebesgue measure on \mathbb{R}^d . Let E be the support of f_0 , i.e. the smallest closed set such that $\int_E f_0 d\mu = 1$, denoting $\text{int}(E)$ the interior of E (the largest open set contained in E) and $\log_+(x) = \max\{\log(x), 0\}$. The following theorem provides a key result to assess the properties of the log-concave maximum likelihood estimator.

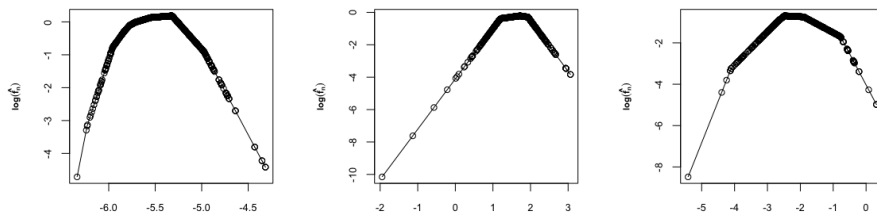


Fig. 3 $\log(\widehat{f}_n)$ for $\log(\ell_{4,k})$ of multifractional random walk (Left), heart rate (Middle) and speed (Right).

Theorem 2 ([69], Theorem 4) Let f_0 be any density on \mathbb{R}^d satisfying

$$\int_{\mathbb{R}^d} \|x\| f_0(x) dx < \infty, \quad \int_{\mathbb{R}^d} f_0 \log_+(f_0) d\mu < \infty \quad \text{and} \quad \text{int}(E) \neq \emptyset.$$

There exists a log-concave density f^* , unique almost everywhere, such that

$$f^* = \underset{f \in \mathcal{F}_0}{\text{argmin}} d_{\text{KL}}(f_0, f), \tag{22}$$

i.e., that minimizes the Kullback-Leibler divergence of f from f_0 over all log-concave densities f .

Let $a_0 > 0$ and $b_0 \in \mathbb{R}$ such that $f^*(x) \leq \exp(-a_0\|x\| + b_0)$; then, for any $a < a_0$,

$$\int_{\mathbb{R}^d} \exp(a\|x\|) |\widehat{f}_n(x) - f^*(x)| dx \rightarrow 0 \quad \text{almost surely as } n \rightarrow \infty, \tag{23}$$

and, if f^* is continuous, then

$$\sup_{x \in \mathbb{R}^d} \exp(a\|x\|) |\widehat{f}_n(x) - f^*(x)| dx \rightarrow 0 \quad \text{almost surely as } n \rightarrow \infty. \quad (24)$$

We can interpret the results of this theorem as follows: when f_0 is log-concave, (23) means that the log-concave maximum likelihood estimator \widehat{f}_n is strongly consistent within specific exponentially weighted total variation metrics, and the convergence is ensured also if $f_0 = f^*$ is continuous (see (24)). The convergence in these exponentially weighted norms provides confidence in the estimator's performance in the extreme tails of the density. When f_0 is not log-concave, there exists a unique log-concave density $f^* \neq f_0$ defined by (22), i.e. that minimizes the Kullback-Leibler divergence from f_0 . Furthermore, the log-concave maximum likelihood estimator \widehat{f}_n converges in the same manner to f^* .

3.2.3 The log-concavity test

In [20], Cule, Samworth, and Stewart investigate the test

$$\mathcal{H}_0 : f \text{ is log-concave} \quad \text{vs} \quad \mathcal{H}_1 : f \text{ is not log-concave.}$$

To address this general problem, they devise a permutation test based on the log-concave maximum likelihood estimator described above. We briefly describe its principle before outlining the steps of the corresponding algorithm.

Consider n random variables X_1, \dots, X_n i.i.d. with density f_0 that we want to test for log-concavity. The random sample is denoted $\mathcal{X} = (X_1, \dots, X_n)$.

Test Principle: The test is based on the Log-Concave Maximum Likelihood Estimator (MLE-LC) defined by (21). The underlying idea is the following:

- If f_0 is truly log-concave, i.e. \mathcal{H}_0 **true**, then \widehat{f}_n applied to the data X_1, \dots, X_n provides a good estimation of f_0 . The test is interpreted as follows: if $d(f_0, \widehat{f}_n)$ is *small*, **we keep** \mathcal{H}_0 .
- If f_0 is not log-concave, i.e. \mathcal{H}_1 **true**, then \widehat{f}_n applied to the data X_1, \dots, X_n converges to some $f^* \neq f_0$ defined by (22) and does not provide a good estimation of f_0 . The test is interpreted as follows: if $d(f_0, \widehat{f}_n)$ is *large*, **we reject** \mathcal{H}_0 .

Test Algorithm:

1. **Fit the MLE-LC** to the data/sample $\mathcal{X} = (X_1, \dots, X_n)$ by using the function `mlelcd` from the package `LogConcDEAD`. This provides a probability density \widehat{f}_n .
2. **Generate** a sample $\mathcal{X}^* = (X_1^*, \dots, X_n^*)$ from \widehat{f}_n by using the function `rlcd` from the package `LogConcDEAD`. This provides n values x_1^*, \dots, x_n^* , which are realizations of n random variables X_1^*, \dots, X_n^* with density \widehat{f}_n .
3. **Compare** the samples $\mathcal{X} = (X_1, \dots, X_n)$ and $\mathcal{X}^* = (X_1^*, \dots, X_n^*)$ by means of the distance

$$T = \sup_{A \in \mathcal{A}_0} |P_n(A) - P_n^*(A)|,$$

where \mathcal{A}_0 is the set of balls centered at a point in $\mathcal{X} \cup \mathcal{X}^*$ and P_n is the empirical distribution associated with \mathcal{X}

$$P_n(A) = \frac{1}{n} \sum_{i=1}^n \delta_{X_i}(A).$$

In the one-dimensional case with realizations x_1, \dots, x_n of X_1, \dots, X_n and x_1^*, \dots, x_n^* of X_1^*, \dots, X_n^* , we consider the test statistic

$$T = \sup_{r>0} \sup_{x \in \{x_1, \dots, x_n, x_1^*, \dots, x_n^*\}} \left| \frac{1}{n} \sum_{i=1}^n \delta_{X_i}((x-r, x+r)) - \delta_{X_i^*}((x-r, x+r)) \right|. \quad (25)$$

4. **”Shuffle the stars”** to increase the test power. Choose a permutation π (uniform random) of $1, \dots, 2n$ to mix the elements of $\mathcal{X} \cup \mathcal{X}^*$ and place stars on the last n elements of the obtained sample

$$x_1, \dots, x_n, x_1^*, \dots, x_n^* \xrightarrow{\pi} x_{\pi(1)}, \dots, x_{\pi(n)}, x_{\pi(n+1)}, \dots, x_{\pi(2n)} =: x_{1,1}, \dots, x_{n,1}, x_{1,1}^*, \dots, x_{n,1}^*.$$

Compute as above

$$T_1^* = \sup_{A \in \mathcal{A}_0} |P_{n,1}(A) - P_{n,1}^*(A)|,$$

where

$$P_{n,1}(A) = \frac{1}{n} \sum_{i=1}^n \delta_{X_{i,1}}(A) \quad \text{and} \quad P_{n,1}^*(A) = \frac{1}{n} \sum_{i=1}^n \delta_{X_{i,1}^*}(A).$$

5. **Repeat the procedure $B - 1$ times:** We obtain T_1^*, \dots, T_B^* . Then, we consider the corresponding order statistics $T_{(1)}^* \leq \dots \leq T_{(B)}^*$.
6. For a level of significance α , we **reject \mathcal{H}_0 if $T > T_{(B+1)(1-\alpha)}^*$** . The test is given by:
 - the test statistic T defined by (25),
 - the rejection region is $T_{(B+1)(1-\alpha)}^*$.

3.2.4 Efficiency of the log-concavity test

To illustrate the performance of the log-concavity test, we compare its results with theoretical expectations using distributions with known properties. Note that while mixtures of log-concave densities can sometimes be log-concave, they generally are not. We use a mixture of standard univariate normal densities $f : x \mapsto \frac{1}{2}\phi(x) + \frac{1}{2}\phi(x-c)$ where ϕ denotes the standard normal density and $\|c\| \in \{0, 2, 4\}$. This mixture is log-concave if and only if $\|c\| \leq 2$. We also examine several parametric families of univariate distributions with log-concave densities, including normal, Gumbel, Laplace, logistic, gamma, and Weibull distributions with a shape parameter of at least one. Additionally, we test the generalized Gaussian distribution, which is log-concave if and only if the shape parameter β satisfies $\beta > 1$. For comparison, we include non-log-concave densities such as Cauchy, Pareto, and lognormal. The log-concavity test was performed on these distributions with a sample size of $n = 200$ and for the log-normal density we used different sizes $n = 200, 500$ and 1000 . The test statistic is

the proportion of rejections out of 100 repetitions, with $B = 99$ and the null hypothesis was rejected with a level of significance $\alpha = 0.05$. The results are summarized in Table 3 below.

Table 3 Empirical rejection probabilities of the log-concavity test (see Subsection 3.2) applied to the usual distribution densities. The sample size is $n = 200$. The rejection proportions lead to the decision (third column) to either retain (LC) the null hypothesis \mathcal{H}_0 that the density is log-concave, to reject it (non-LC), or to neither reject nor retain \mathcal{H}_0 (inconclusive). The last column indicates whether (based on known theoretical results) the density is truly log-concave or not.

Density		Prop. of reject \mathcal{H}_0	Decision	Theoretical result
$f(x) = \frac{1}{2}\phi(x) + \frac{1}{2}\phi(x - c)$	$c = 0$	0.03	LC	LC
	$c = 2$	0.02	LC	LC
	$c = 4$	0.29	Inconclusive	Non LC
Gumbel: $f(x, 1, 1) = e^{e^{1-x}}$		0.02	LC	LC
Laplace (0,1): $f(x) = \frac{1}{2}e^{- x }$		0	LC	LC
Logistic: $f(x, 0, 1) = \frac{e^{-x}}{(1 + e^{-x})^2}$		0	LC	LC
Gamma: $f(x, 1, 2) = \frac{1}{2\Gamma(1)}e^{-x/2}$		0.01	LC	LC
Weibull: $f(x, 2, 2) = \frac{x}{2}e^{-x^2/4}$		0.01	LC	LC
Cauchy: $f(x, 0, 1) = \frac{1}{\pi} \frac{1}{x^2 + 1}$		1	Non LC	Non LC
Pareto: $f(x, 1, 1) = \frac{1}{x^2}$		1	Non LC	Non LC
Generalized Gaussian: $f(x) = \frac{\beta e^{- x ^\beta}}{2\Gamma(1/\beta)}$	$\beta = 0.5$	0.93	Non LC	Non LC
	$\beta = 1.5$	0	LC	LC
Lognormal: $f(x) = \frac{1}{x\sqrt{2\pi}}e^{-\frac{\log^2(x)}{2\sigma^2}}$	$n = 200$	0.06	LC	Non LC
	$n = 1000$	0.37	Inconclusive	Non LC

Table legend: LC: log-concave, Non LC: non log-concave.

In light of the results reported in Table 3, it is clear that the test is effective and, in most cases, the outcomes align with the nature of each distribution. When the decisions to reject or not reject the null hypothesis \mathcal{H}_0 do not align with whether the underlying density is truly log-concave or not, it is worth noting that the test can still detect a significant departure from log-concavity. In this case, the rejection rate is too high ($\gg 5\%$) for us to retain \mathcal{H}_0 with confidence, which leads to the decision to neither reject nor retain \mathcal{H}_0 (indicated in the table as *inconclusive*). This occurs in the log-concave case with $n = 1000$, where a larger sample allows for contradicting the incorrect 'LC' decision obtained with $n = 200$ test runs. Similarly, in the case of

a mixture with $c = 4$, the high rejection rate suggests running the test on a larger sample (see experiments with different sample sizes in Cule and Samworth [69]) to refine the result and ultimately reject \mathcal{H}_0 .

3.2.5 Application of the log-concavity test to log-leaders

Table 4 Log-concavity test on log-leaders $\log(\ell_{j,k})$, where $j \in \{4, 5, 6\}$, for different processes and real data. The test result shows the proportion of times out of 100 repetitions that the null hypothesis \mathcal{H}_0 was rejected.

	X	$\log(\ell_{4,k})$	$\log(\ell_{5,k})$	$\log(\ell_{6,k})$
fBm	$H = 0.4$	0.01	0.18	0.02
	$H = 0.7$	0.00	0.13	0.02
	CMC-motion	0.01	0.02	0.02
	CPM-LN	0.05	0.05	0.02
	CPM-LP	0.00	0.00	0.00
	MRW	0.02	0.04	0.03
	Heart rate	0.08	0.04	0.04
	Speed	0.17	0.06	0.02

We use the same processes and real data as in Section 3.1.1 to perform the log-concavity test on log-leaders. The results in Table 4 clearly show that the proportion of times the null hypothesis was rejected out of 100 repetitions is very low. This confirms that the log-concavity of the distribution of log-leaders is a realistic hypothesis. This is an encouraging result, especially when working with real data where no theoretical properties are known. Given the practical implications of this finding, it would be valuable to validate this hypothesis across a broader range of real life datasets. Testing the log-concavity of log-leaders on different types of data, drawn from various fields such as finance, biology, or physics, would not only strengthen the generalizability of this hypothesis but also reveal its potential limitations.

A relevant question to address is the effect of changing the mother wavelet ψ on the results of the log-concavity test of the log-leaders. To explore this, using the example of the Multifractal Random Walk (with the same parameters as in Section 3.1.1), we choose to apply the test with two wavelet bases that differ significantly in both regularity and support size, specifically Daubechies wavelets with varying numbers of vanishing moments: $N_\psi = 1$ corresponding to the Haar wavelet, and $N_\psi = 4$. Notably, a smaller N_ψ corresponds to a more irregular wavelet with smaller support. The results of the log-concavity test on the log-leaders, shown in Table 5, indicate that the choice of wavelet does not affect the test outcomes. Indeed, the proportion of times the null hypothesis was rejected across 100 repetitions remains consistently low, reinforcing the potential validity of the log-concavity hypothesis for the distribution of log-leaders.

This example indicates that the test results are robust to changes in the choice of the wavelet basis. In other words, the log-leaders appear to maintain their log-concavity regardless of the wavelet basis's characteristics, such as its regularity and support. However, while this result of robustness is promising, it is only based on numerical evidence and a thorough theoretical study would be needed to support these findings in all generality.

Table 5 Log-concavity test on log-leaders $\log(\ell_{j,k})$, where $j \in \{4, 5, 6\}$, for a multifractal random walk (MRW) using Daubechies wavelets with different vanishing moments $N_\psi = 1$ and $N_\psi = 4$. The test result shows the proportion of times out of 100 repetitions that the null hypothesis \mathcal{H}_0 was rejected.

Wavelet	$\log(\ell_{4,k})$	$\log(\ell_{5,k})$	$\log(\ell_{6,k})$
$N_\psi = 1$	0.01	0.00	0.03
$N_\psi = 4$	0.01	0.12	0.00

4 Estimation of multifractality parameters

In this section, we focus on estimating two important multifractality parameters: c_1 and c_2 (we leave the statistical estimation of the third major multifractality parameter and H_f^{min} for the forthcoming article [19]). An estimator for the coefficients c_1 and c_2 was introduced by Jacyna et al. [70] and comes with theoretical guarantees through confidence intervals. We examine the assumptions underlying its applicability by leveraging the analysis of log-leader distributions presented in Section 3.

4.1 Estimation of c_1 and c_2

In this section, we revisit the estimation procedure for c_1 and c_2 developed in Jacyna et al. [70], questioning the assumptions of its application. Consider a process $X = (X(t))_{t \in \mathbb{R}_+} \in L_{\text{loc}}^\infty(\mathbb{R}^d)$ whose wavelet coefficients are defined by (5) and wavelet leaders by (6). Recalling (17) the coefficients c_1 and c_2 are defined by the equations

$$C_1(j) = c_{0,1} + c_1 \log(2^{-j}) \quad \text{and} \quad C_2(j) = c_{0,2} + c_2 \log(2^{-j}). \quad (26)$$

where for $m \in \{1, 2\}$, $C_m(j)$ denotes the m -th order cumulant of the random variables $\log(\ell_{j,k})$. Consider N i.i.d. copies X^1, \dots, X^N of the process X and M scales j_1, \dots, j_M . This leads to define the estimates $(\hat{c}_{0,1}^{(i)}, \hat{c}_1^{(i)})$ and $(\hat{c}_{0,2}^{(i)}, \hat{c}_2^{(i)})$ by the equations

$$\hat{c}_{0,1}^{(i)} + \hat{c}_1^{(i)} \log(2^{-j}) = \frac{1}{n_j} \sum_{k=1}^{n_j} \log(\ell_{j,k}^{(i)}) =: \hat{\mu}_j^{(i)}$$

$$\text{and } \widehat{c}_{0,2}^{(i)} + \widehat{c}_2^{(i)} \log(2^{-j}) = \frac{1}{n_j} \sum_{k=1}^{n_j} \left(\log(\ell_{j,k}^{(i)}) - \widehat{\mu}_j^{(i)} \right)^2 =: \widehat{\sigma}_j^{(i)}. \quad (27)$$

where, for any $j \in \{j_1, \dots, j_M\}$, n_j stands for the number of translations k at scale j . For any $i \in \{1, \dots, N\}$, we define the vectors $\widehat{\boldsymbol{\mu}}^{(i)} = (\widehat{\mu}_{j_1}^{(i)}, \dots, \widehat{\mu}_{j_M}^{(i)})$ and $\widehat{\boldsymbol{\sigma}}^{(i)} = (\widehat{\sigma}_{j_1}^{(i)}, \dots, \widehat{\sigma}_{j_M}^{(i)})$. The least-squares estimates $\widehat{\mathbf{c}}_1^{(i)} := (\widehat{c}_{0,1}^{(i)}, \widehat{c}_1^{(i)})$ and $\widehat{\mathbf{c}}_2^{(i)} := (\widehat{c}_{0,2}^{(i)}, \widehat{c}_2^{(i)})$ can be rewritten as

$$\widehat{\mathbf{c}}_1^{(i)} = (\widehat{c}_{0,1}^{(i)}, \widehat{c}_1^{(i)}) := (\mathbf{H}^\top \mathbf{H})^{-1} \mathbf{H}^\top \widehat{\boldsymbol{\mu}}^{(i)} \quad \text{and} \quad \widehat{\mathbf{c}}_2^{(i)} = (\widehat{c}_{0,2}^{(i)}, \widehat{c}_2^{(i)}) := (\mathbf{H}^\top \mathbf{H})^{-1} \mathbf{H}^\top \widehat{\boldsymbol{\sigma}}^{(i)}, \quad (28)$$

where the matrix \mathbf{H} is given by

$$\mathbf{H} = \begin{pmatrix} 1 & \log(2^{-j_1}) \\ 1 & \log(2^{-j_2}) \\ \vdots & \vdots \\ 1 & \log(2^{-j_M}) \end{pmatrix}.$$

We consider then the estimators

$$\begin{aligned} \widehat{\mathbf{c}}_1 &:= (\widehat{c}_{0,1}, \widehat{c}_1) := \frac{1}{N} \sum_{i=1}^N \widehat{\mathbf{c}}_1^{(i)} = \frac{1}{N} \sum_{i=1}^N (\mathbf{H}^\top \mathbf{H})^{-1} \mathbf{H}^\top \widehat{\boldsymbol{\mu}}^{(i)} \\ \text{and } \widehat{\mathbf{c}}_2 &:= (\widehat{c}_{0,2}, \widehat{c}_2) := \frac{1}{N-1} \sum_{i=1}^N \widehat{\mathbf{c}}_2^{(i)} = \frac{1}{N-1} \sum_{i=1}^N (\mathbf{H}^\top \mathbf{H})^{-1} \mathbf{H}^\top \widehat{\boldsymbol{\sigma}}^{(i)}. \end{aligned} \quad (29)$$

By definition, $C_1(j) = \mathbb{E}[\log(\ell_{j,k})] =: m_j$ for all $j \in \{j_1, \dots, j_M\}$, and letting $\mathbf{m} = (m_1, \dots, m_M)$, it follows that $\mathbb{E}[\widehat{\mathbf{c}}_1] = (\mathbf{H}^\top \mathbf{H})^{-1} \mathbf{H}^\top \mathbf{m} = (c_{0,1}, c_1) =: \mathbf{c}_1$. Therefore, $\widehat{\mathbf{c}}_1$ is an unbiased estimator of $\mathbf{c}_1 := (c_1, \dots, c_1) \in \mathbb{R}^N$. A similar argument shows that $\widehat{\mathbf{c}}_2$ is an unbiased estimator of \mathbf{c}_2 .

Expanding (28), we get

$$\widehat{c}_1^{(i)} = \sum_{k=1}^M (\mathbf{h}_{2,1} + \mathbf{h}_{2,2} \log(2^{-j_k})) \widehat{\mu}_{j_k}^{(i)} \quad (30)$$

by writing $(\mathbf{H}^\top \mathbf{H})^{-1} = (\mathbf{h}_{i,j})_{(i,j) \in \{1,2\}^2}$.

Assuming that the log-leader distributions are log-concave (an hypothesis empirically validated in Section 3), the random variables $\log(\ell_{j,k})$ have finite moments of all orders, including a finite variance. By the Central Limit Theorem (CLT),

$$Z_N := \sqrt{N} \frac{(\widehat{c}_1 - c_1)}{\sigma_{c_1}} \xrightarrow[N \rightarrow \infty]{\mathcal{L}} \mathcal{N}(0, 1), \quad (31)$$

where σ_{c_1} is the common standard deviation of the $\widehat{c}_1^{(i)}$. From this, we derive the confidence interval (valid for $N \geq 30$):

$$c_1 \in \left[\widehat{c}_1 - z_{\alpha/2} \frac{\widehat{\sigma}_{c_1}}{\sqrt{N}}, \widehat{c}_1 + z_{\alpha/2} \frac{\widehat{\sigma}_{c_1}}{\sqrt{N}} \right],$$

where $\widehat{\sigma}_{c_1}$ is the empirical estimator of σ_{c_1} and $z_{\alpha/2}$ is the $(1 - \alpha/2)$ -quantile of the Normal distribution, corresponding to the desired confidence level $1 - \alpha$. The quality of the normal approximation provided by the Central Limit Theorem (31) can be assessed using the Berry-Esseen theorem, which states that

$$\sup_{x \in \mathbb{R}} |\mathbb{P}(Z_N \leq x) - \Phi(x)| \leq \frac{C}{c_2^{3/2} N^{3/2}} \sum_{i=1}^N \mathbb{E}[|\widehat{c}_1^{(i)} - c_1|^3],$$

where C is some constant smaller than 0.46 (see [71]). Note that by (30) we get

$$\mathbb{E}[|\widehat{c}_1^{(i)} - c_1|^3] = \sum_{k=1}^M (\mathbf{h}_{2,1} + \mathbf{h}_{2,2} \log(2^{-j_k})) \mathbb{E}[|\widehat{\mu}_{j_k}^{(i)} - m_k|^3] < \infty,$$

since the third absolute moment is always finite due to the exponential (or faster) decay of the tails of log-concave distributions. We thus recover the estimation results and a confidence interval for the estimates of c_1 and c_2 stated in Jacyna et al. [70], without relying on the assumption that the log-leaders form a stationary Gaussian field, as assumed in their work and refuted in Subsection 3.1.2.

4.2 Numerical experiments

Procedure: We consider two types of processes with different multifractal properties (described in Section 3.1.1). The first is fractional Brownian motion (fBm), a monofractal process, where the parameter c_1 coincides with the Hurst exponent H , and $c_2 = 0$. The second is the Multifractal Random Walk (MRW), a multifractal process, for which c_1 is given by $c_1 = H + \beta^2/2$ and $c_2 = -\beta^2$. For the numerical study, we simulate $N = 100$ realizations of each stochastic process, with a sample size of 1310, uniformly sampled over the time interval $[0, 1]$. Estimation is performed using Daubechies wavelets with $N_\psi = 3$ vanishing moments, and the choice of scales (j_1, \dots, j_M) is described below.

Tuning Parameter To describe the scale selection procedure, we consider $N = 100$ simulations of fBm with $H = 0.8$. Performing a multifractal analysis for each process, we examine the log-log regression used to estimate the parameter h_{\min} , which corresponds to the uniform regularity of the function in the scale provided by global Hölder spaces (see Figure 4). Numerically, it is determined as the slope of the linear regression between the scales and the logarithm of the supremum of the wavelet coefficients at each scale. This choice of regression is justified as it provides a robust estimate of this classification parameter (see [25]).

We extract the range of scales that yields the best linear regression fit, based on the

coefficient of determination, denoted R^2 . The coefficient R^2 measures the goodness of fit of the regression, with values closer to 1 indicating a stronger linear relationship between the variables. It is defined as

$$R^2 = 1 - \frac{\sum_i (y_i - \hat{y}_i)^2}{\sum_i (y_i - \bar{y})^2},$$

where y_i represents the observed values, \hat{y}_i the predicted values from the regression model, and \bar{y} the mean of the observed values. After N simulations, we select the most frequently occurring scale range $\{j_1, \dots, j_M\}$ and use it for the estimation of the multifractal parameters c_1 and c_2 , see Figure 4.

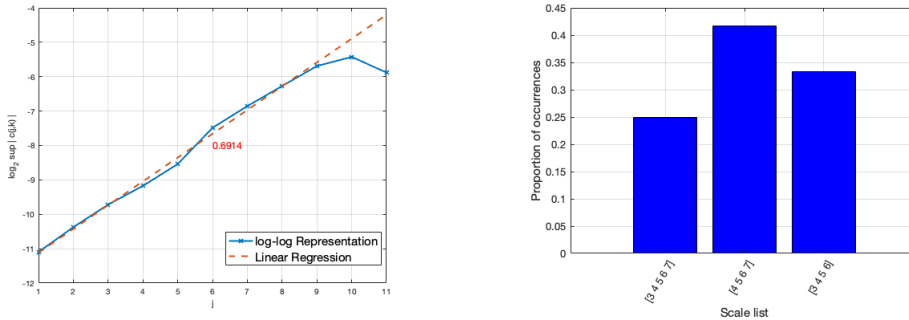


Fig. 4 Left, log-log plot illustrating the linear regression performed to estimate h_{min} for a fractional Brownian motion with Hurst parameter $H = 0.8$. Right, histogram displaying the proportion of occurrences of the different scale intervals selected as yielding the optimal linear regression across $N = 100$ independent realizations.

Results and interpretation: In Table 6, we present the confidence intervals for the parameter c_1 for different realizations of fBm and MRW, choosing $H \in \{0.5, 0.6, 0.7, 0.8, 0.9\}$ and setting $\beta = 0.1$. In each case, we compare the confidence intervals (95% confidence level, $\alpha = 0.05$) obtained with those estimated using the percentile bootstrap method, see [14, 34, 35, 72]. The percentile bootstrap method is a non-parametric approach for constructing confidence intervals without assuming a specific distribution for the data. It relies on resampling with replacement from the original dataset to generate B bootstrap samples. For each sample, the parameter of interest is estimated, denoted by $\hat{\theta}_b$. The empirical distribution of these bootstrap estimates is then used to determine the α quantiles $\hat{\theta}_\alpha$ corresponding to the desired confidence level. Thus, the confidence interval at level $1 - \alpha$ is

$$CI_{\theta, (1-\alpha)}^{\text{Per}} = \left[\hat{\theta}_{\frac{\alpha}{2}}, \hat{\theta}_{1-\frac{\alpha}{2}} \right].$$

Thus, for the bootstrap method, we adopt a sample size of 131000, ensuring that any differences in confidence interval widths are attributable to the intrinsic properties of the estimation techniques rather than disparities in sample size. Thus, the comparison of confidence intervals highlights that those obtained using our CLT-based

estimation method generally have smaller widths than the bootstrap-derived intervals. This reduction in interval width suggests that our approach provides a more precise estimation of the parameter c_1 , thereby enhancing statistical efficiency. While the bootstrap method tends to yield slightly wider intervals, reflecting a more conservative quantification of uncertainty, the difference remains moderate, ensuring that both methods offer consistent inference. The narrower confidence intervals obtained via the CLT-based approach indicate its potential advantage in terms of precision, while the bootstrap method remains a robust alternative, particularly useful in scenarios where parametric assumptions may not hold. These findings demonstrate the effectiveness of our method in providing refined estimates while maintaining coherence with an established resampling technique. Table 7 presents the estimates of the c_2 coefficient for fBm and MRW models across different values of $H \in \{0.5, 0.6, 0.7, 0.8, 0.9\}$ and fixed $\beta = 0.1$. The theoretical value of c_2 is 0 for fBm and -0.01 for MRW. Three estimation methods are compared: our proposed CLT-based method \hat{c}_2 , the percentile bootstrap estimator \hat{c}_2^b , and the Bayesian estimator \hat{c}_2^{BY} which is based on the assumption of the normality of log-leaders, see [16, 17, 38]. For both the fBm and MRW models, the CLT-based estimator consistently provides the most reliable estimates, yielding results that are closest to the theoretical values. This method demonstrates stability and precision, with minimal deviations across all values of the Hurst exponent. In contrast, the bootstrap estimator exhibits higher variability, leading to less accurate estimates. For instance, in the MRW model with $H = 0.7$, the bootstrap estimator produces a value of $\hat{c}_2^b = -0.039$, which deviates significantly from the theoretical value of -0.01 . Meanwhile, the Bayesian estimator provides reasonably accurate results for MRW, but its estimates exhibit more fluctuation compared to the CLT-based method. These findings highlight the CLT-based method as the most accurate and stable for estimating c_2 , consistently yielding values closest to the truth, especially for MRW. In contrast, the bootstrap and Bayesian methods show greater variability and slightly lower precision.

Conclusion: The CLT-based estimator offers comparable precision to other methods for estimating c_1 and c_2 but stands out for its weaker assumption—requiring only log-concavity of the log-leaders. Additionally, it is significantly faster, with a runtime of approximately 14 seconds, comparable to the Bayesian method, and nearly five times shorter than the bootstrap method, which takes about 1 minute and 10 seconds.

5 Theoretical study of the distribution of log-leaders for random wavelet series

Previous statistical tests (see Section 3) provided a broad understanding of the distribution of log-leaders: they are not normally distributed, but their distribution appears to be log-concave. To illustrate these experimental findings, we provide a first attempt to study the distribution of the log-leaders associated to *random wavelet series* $X = (X(t))_{t \in \mathbb{R}_+}$ defined by

$$X(t) = \sum_{j,k} 2^{-\alpha j} X_{j,k} \psi(2^j t - k), \quad (32)$$

Table 6 Confidence intervals for the parameter c_1 for fractional Brownian motion (fBm) and Multifractal Random Walk (MRW) with the same sample size, considering different values of Hurst parameter $H \in \{0.5, 0.6, 0.7, 0.8, 0.9\}$ and fixed $\beta = 0.1$. Two estimation methods are compared: our proposed CLT-based method (CLT method) and the percentile bootstrap method (Bootstrap) with $B = 100$ bootstrap samples, both at 95% confidence level ($\alpha = 0.05$). The columns **LB** and **UB** denote the lower and upper bounds of the confidence intervals, respectively, while **UB-LB** represents the interval width.

fBm						
Theoretical c_1	CLT method			Bootstrap		
	LB	UB	UB-LB	LB	UB	UB-LB
0.5	0.4709	0.5071	0.0362	0.485	0.532	0.047
0.6	0.5811	0.6076	0.0265	0.584	0.606	0.022
0.7	0.6845	0.7161	0.0316	0.6808	0.7152	0.0344
0.8	0.7842	0.8126	0.0284	0.773	0.823	0.05
0.9	0.89	0.9197	0.0297	0.87	0.931	0.061

MRW						
Theoretical c_1	CLT method			Bootstrap		
	LB	UB	UB-LB	LB	UB	UB-LB
0.505	0.4641	0.5052	0.0411	0.464	0.508	0.044
0.605	0.5784	0.6055	0.0271	0.585	0.617	0.032
0.705	0.681	0.7102	0.0292	0.696	0.734	0.038
0.805	0.7938	0.8292	0.0354	0.8	0.85	0.05
0.905	0.8693	0.9224	0.0531	0.88	0.937	0.057

Table 7 Estimates of the c_2 parameter for fractional Brownian motion (fBm) model ($c_2 = 0$) and the multifractal random walk (MRW) model ($c_2 = -0.01$), for different values of Hurst exponent $H \in \{0.5, 0.6, 0.7, 0.8, 0.9\}$ and fixing $\beta = 0.1$. The estimates are obtained using our proposed CLT-based method (\hat{c}_2), the percentile bootstrap method (\hat{c}_2^b) ($B=100$), and the Bayesian method (\hat{c}_2^{BY}). Bold values indicate the negative estimates closest to the theoretical values.

fBm $c_2 = 0$				MRW $c_2 = -0.01$			
H	\hat{c}_2	\hat{c}_2^b	\hat{c}_2^{BY}	H	\hat{c}_2	\hat{c}_2^b	\hat{c}_2^{BY}
0.5	-0.0118	0.008	-0.0036	0.5	-0.01	-0.018	-0.0127
0.6	-0.0001	-0.004	-0.0051	0.6	-0.0084	-0.017	-0.0152
0.7	-0.004	-0.004	-0.0049	0.7	-0.0113	-0.039	-0.0159
0.8	-0.002	0.002	-0.0066	0.8	-0.0155	-0.018	-0.0172
0.9	-0.001	0.011	-0.0074	0.9	-0.0104	-0.006	-0.0183

where $\alpha \in \mathbb{R}_+^*$, the $2^{j/2}\psi(2^j \cdot + k)$ ($j, k \in \mathbb{Z}$) form an orthonormal wavelet basis and the wavelet coefficients satisfy the following assumptions (see [73] and therein):

- The wavelet coefficients are independent both *within* and *across* scales,

- The random variables $X_{j,k}$ appearing in (32) are generalized Gaussians, i.e. their common density is defined on \mathbb{R} by

$$f_\beta(x) = \frac{\beta}{2\Gamma(\frac{1}{\beta})} e^{-|x|^\beta} =: \kappa_\beta e^{-|x|^\beta}, \quad (33)$$

where Γ denotes the gamma function, $\beta > 0$ is the shape parameter and $\kappa_\beta > 0$ is a normalizing constant which belongs to the interval $(0, 0.565)$ for any $\beta > 0$. The family of densities $\{f_\beta, \beta > 0\}$ includes the normal distribution (with variance $1/2$) when $\beta = 2$ and the Laplace distribution when $\beta = 1$.

We justify the assumption that the variables are generalized Gaussians rather than standard Gaussians based on considerations from signal and image processing [74], where such model assumptions are derived from the inspection of large collections of data. In these fields, wavelet coefficients often exhibit non-Gaussian distributions: most are small, but a few have large magnitudes, leading to heavy-tailed distributions when $\alpha < 2$ [29]. Bayesian estimation methods have integrated non-Gaussian priors using Gaussian Mixture Models (GMM) [75], a mixture of a Gaussian and a point mass at 0 [76], and Gaussian scale mixtures for image denoising [28, 77].

Remark 1 To streamline the computations, we assume in this section that the wavelet coefficients are independent both *across* and *within* scales, meaning that the $X_{j,k}$ are independent in both j and k . This brief analysis aims to theoretically validate the log-concavity model of log-leaders proposed in this paper, while recognizing that it relies on the widely used yet restrictive assumption of independence between scale coefficients. We also justify neglecting these dependencies because we propose to provide an approximation rather than an exact form of the log-leaders' law. The long-term objective is to explore the implications that scale dependencies have on the laws of log-leaders; part of this program is developed in the forthcoming paper [19].

The previous assumptions entail a simplified model of a continuous law exhibiting non-zero density in the vicinity of 0. We identify the pair (j, k) and $\lambda := \lambda_{j,k} := [k/2^j, (k+1)/2^j]$ and we define the leaders as

$$\ell_{j,k}^1 = \ell_\lambda^1 = \sup_{\lambda' \subset \lambda} |c_{\lambda'}|. \quad (34)$$

Note that we do not use $\lambda' \subset 3\lambda$ to guarantee independence between leaders at the same scale, despite its advantages in facilitating theoretical results and improving numerical efficiency. However, the standard proof establishing that the Legendre spectrum provides an upper bound for the multifractal spectrum, see [24], relies on a definition of the scaling function based on 3-leaders, as given in (6), i.e., with the quantity

$$\ell_{j,k}^3 = \ell_\lambda^3 = \sup_{\lambda' \subset 3\lambda} |c_{\lambda'}|,$$

see (10); in order to validate our simplifying choice here, it is therefore important to verify that the definitions of scaling functions using either ℓ_λ^1 or ℓ_λ^3 actually coincide.

Let us introduce the following notations: we define the corresponding wavelet leader structure functions

$$\text{for } i \in \{1, 3\}, \quad j \geq 0, \quad \text{and } \forall q \in \mathbb{R}, \quad S_i(j, q) = 2^{-dj} \sum_k |\ell_{j,k}^i|^q,$$

and the leader scaling functions as

$$\text{for } i \in \{1, 3\}, \quad \forall q \in \mathbb{R}, \quad \zeta_i(q) = \liminf_{j \rightarrow +\infty} \frac{\log(S_i(j, q))}{\log(2^{-j})}.$$

Proposition 3 *For any locally bounded function, the two leader scaling functions defined above coincide, i.e.*

$$\forall q \in \mathbb{R}, \quad \zeta_1(q) = \zeta_3(q). \quad (35)$$

Proof This result is proved in Appendix A. □

Remark 2 At a given scale j , all leaders $\ell_{j,k}^1$ share the same distribution, and the distributions across scales can be derived from $\ell_{0,0}^1$ by rescaling with the factor $2^{-\alpha j}$. Hence, it is sufficient to determine the distribution of $\ell_{0,0}^1$. We denote $I := \lambda_{0,0} = [0, 1]$.

Under previous assumptions, we are led to compute

$$\begin{aligned} \mathbb{P}(\ell_{0,0}^1 \leq A) &= \mathbb{P}\left(\sup_{\lambda \subset I} |c_\lambda| \leq A\right) \\ &= \prod_{(j,k): \lambda \subset I} \mathbb{P}(|c_{j,k}| \leq A) \\ &= \prod_{(j,k): \lambda \subset I} \mathbb{P}(|X_{j,k}| \leq 2^{\alpha j} A) \end{aligned} \quad (36)$$

$$= \prod_{j \in \mathbb{N}} \mathbb{P}(|X_{j,k}| \leq 2^{\alpha j} A)^{2^j}, \quad (37)$$

where we have used the independence of the $c_{j,k}$ in the second line and that the $X_{j,k}$ are identically distributed in the last one. We are interested in the tail regime, specifically when A takes very small or very large values for two main reasons:

- **Relevance to Applications:** As detailed in Section 2.3 examining small values of A is particularly relevant for applications. In such cases, wavelet leaders are preferred over wavelet coefficients as multiresolution quantities in scaling functions. This preference arises because, unlike wavelet coefficients, the distributions of wavelet leaders vanish near zero, enabling the reliable numerical computation of negative moments which, in some applications yields a key information on the decreasing part of the multifractal spectrum. The computations presented here represent the first mathematical effort to rigorously substantiate this claim.

- **Exponential Decay of Tails:** Log-concave distributions are defined by tails that decay at least as rapidly as exponential distributions. While the explicit asymptotic results we obtain cannot definitively confirm or refute the log-concavity of the distributions of log-leaders, they do show that the tails of these distributions decay exponentially fast. This finding is consistent with the hypothesis of log-concavity tested in the previous section.

The following approximation results yield the tail distributions of log-leaders.

Theorem 4 *let $X = (X(t))_{t \in \mathbb{R}_+}$ denote the random wavelet series defined by (32) where the distribution of the $X_{j,k}$ is given by (33); then the following results hold:*

1. **Distribution of small leaders** *Assume that $\alpha > \log(1.13\pi)/\log 4 \simeq 0.914$. Let $A \leq 2^{-\alpha}$. Then, there exist constants $\lambda_1, \lambda_2 > 0$ such that*

$$\lambda_1 \frac{2^\alpha}{A} \exp\left(A^{-1/\alpha} \log\left(\frac{2c_{l_\beta} \kappa_\beta \Lambda_\beta}{2^{2\alpha}}\right)\right) \leq \mathbb{P}(\ell_{0,0}^1 \leq A) \leq \lambda_2 \frac{2^\alpha}{A} \exp\left(A^{-1/\alpha} \log\left(\frac{2c_{l_\beta} \kappa_\beta \Lambda_\beta}{2^{2\alpha}}\right)\right), \quad (38)$$

where

$$c_{l_\beta} = \prod_{j \geq l_\beta} (1 - 1/(4j^2)),$$

$l_\beta > 0$ is a constant, κ_β and $\Lambda_\beta \in (1, \pi/2)$ are given by (33) and (48), respectively.

2. **Distribution of large leaders.** *Assume that α satisfies $2^{\alpha\beta}(1/\log(2) - \alpha\beta + \log_2(\alpha\beta \log(2))) - 1 > 0$. For any $\beta > 0$ there exist A_β and $C_{\alpha,\beta} > 0$ such that for all $A > A_\beta$,*

$$\mathbb{P}(\ell_{0,0}^1 > A) \leq \frac{C_{\alpha,\beta} e^{-A^\beta}}{\beta A^{\beta-1}}. \quad (39)$$

Case 1: *If $\beta > 1$, then A_β can be chosen such that*

$$\frac{1}{1 + (\beta - 1)/(\beta A_\beta^\beta)} = 0.99.$$

Case 2: *If $0 < \beta < 1$, then A_β can be chosen such that*

$$\frac{1}{1 - (1 - \beta)/(\beta A_\beta^\beta)} = 1.01.$$

Case 3: $\beta = 1$. *If A is chosen large enough so that $\forall j \in \mathbb{N}, 2^{\alpha j} A \geq A + 2^{\alpha j}$, then*

$$\mathbb{P}(\ell_{0,0}^1 > A) \leq e^{-j2^\alpha} = e^{-A} \frac{1}{1 - \frac{2}{e^{2^\alpha A}}}.$$

Remark 3 (Conditions on α) For technical reasons and to facilitate calculations, we impose conditions on the value of α that depend on whether we are analyzing the distribution of small or large leaders.

The function $\beta \in \mathbb{R}_+^* \mapsto \kappa_\beta = \beta/\Gamma(1/\beta)$ is bounded by 1.13. Consequently, when considering small leaders, we choose

$$\alpha > \log(1.13\pi)/\log 4 \simeq 0.914.$$

Indeed, since $c_{l_\beta} \in (2/\pi, 1)$ and $\Lambda_\beta \in (1, \pi/2)$, we obtain

$$2\alpha \log 2 > \log(1.13\pi) > \log(2c_{l_\beta} \kappa_\beta \Lambda_\beta). \quad (40)$$

For large leaders, we consider the function $g_c : x \in \mathbb{R}^+ \mapsto 2^{cx} - 2^c x - 1$ for any $c > 0$. It can be shown that if $g(x_c) > 0$, where

$$x_c = \frac{2^c}{\log 2} - c + \log_2(c \log 2),$$

then g_c remains positive over \mathbb{R}_+ . Let $c = \alpha\beta$. Assuming that α satisfies $x_{\alpha\beta} > 0$, we further have that for any $j \geq 0$, $e^{-(2^{\alpha j} A)^\beta} \leq e^{-A^\beta} e^{-j(2^\alpha A)^\beta}$, which is useful for computations.

Remark 4 (Order of distribution tails) It follows from (38) and (40) that

$$\mathbb{P}(\ell_{0,0}^1 \leq A) = \Theta(A^{-1} \exp(-c_{\alpha,\beta} A^{-1})),$$

where for two real functions f and g , $f(A) = \Theta(g(A))$ means that f grows asymptotically (with respect to A) at the same rate as g ; and $c_{\alpha,\beta} = 2\alpha \log 2 - \log(2c_{l_\beta} \lambda_\beta \kappa_\beta)$ is a constant which does not depend on A . The tail of the distribution for small log-leaders is exponential, while the factor A^{-1} corresponds to a logarithmic correction. Equation (39) shows that the tails of large leaders also exhibit exponential decay. Both tail behaviors of large and small leaders are consistent with the properties of log-concave distributions, which exhibit exponential or sub-exponential decay.

The proof of Theorem 4 relies on Lemma 1 (see Appendix B). We will also use the following well-known identities

$$\sum_{k=0}^N kx^k = \frac{x(Nx^{N+1} - (N+1)x^N + 1)}{(x-1)^2}, \quad (41)$$

that holds for any $N \in \mathbb{N}^*$ and $x \in \mathbb{R}$, as well as

$$\prod_{j \in \mathbb{N}^*} \left(1 - \frac{1}{4j^2}\right) = \frac{2}{\pi} \quad \text{and} \quad \prod_{j \in \mathbb{N}^*} \left(1 + \frac{1}{4j(j+1)}\right) = \frac{4}{\pi}. \quad (42)$$

Proof of Theorem 4 **Distribution of small leaders** Let some $\alpha > \log(1.13\pi)/\log 4$. Assuming that $A \leq 2^{-\alpha}$, there exists $l \in \mathbb{N}^*$ such that $2^{-\alpha(l+1)} < A \leq 2^{-\alpha l}$. For t small enough,

$$\mathbb{P}(|X_{j,k}| \leq t) = \kappa_\beta \int_{-t}^t e^{-|x|^\beta} dx \underset{t}{\sim} \kappa_\beta \int_{-t}^t dx = 2\kappa_\beta t,$$

where the symbol \sim indicates that the functions are equivalent in the limit when $t \rightarrow 0$. Then,

$$\prod_{j \in \mathbb{N}} \mathbb{P}(|X_{j,k}| \leq 2^{\alpha j} A)^{2^j} \leq \prod_{j=0}^{l-1} \mathbb{P}(|X_{j,k}| \leq 2^{\alpha(j-l)})^{2^j} \prod_{j \geq l} \mathbb{P}(|X_{j,k}| \leq 2^{\alpha(j-l)})^{2^j}$$

$$\begin{aligned}
& \sim (2\kappa_\beta)^{2^l-1} \prod_{j=0}^{l-1} 2^{-2^j \alpha(l-j)} \prod_{j \geq l} \mathbb{P}(|X_{j,k}| \leq 2^{\alpha(j-l)})^{2^j} \\
& = (2\kappa_\beta)^{2^l-1} \cdot 2^{-\alpha \sum_{j=0}^{l-1} 2^j(l-j)} \prod_{j \geq l} \mathbb{P}(|X_{j,k}| \leq 2^{\alpha(j-l)})^{2^j} \\
& = (2\kappa_\beta)^{2^l-1} \cdot 2^{-\alpha(2^{l+1}-(l+2))} \prod_{j \geq l} \mathbb{P}(|X_{j,k}| \leq 2^{\alpha(j-l)})^{2^j} \\
& = (2\kappa_\beta)^{2^l-1} \cdot 2^{-\alpha(2^{l+1}-(l+2))} \prod_{i \geq 0} \mathbb{P}(|X_{i,k}| \leq 2^{\alpha i})^{2^{i+l}}, \quad (43)
\end{aligned}$$

where (41) was used in the third line with $x = 1/2$ to show that

$$\sum_{j=0}^{l-1} 2^j(l-j) = 2^l \sum_{k=1}^l k 2^{-k} = 2^l \cdot 2(l 2^{-(l+1)} - (l+1)2^{-l} + 1) = 2^{l+1} - (l+2).$$

Similarly, we can check that

$$\prod_{j \in \mathbb{N}} \mathbb{P}(|X_{j,k}| \leq 2^{\alpha j} A)^{2^j} > (2\kappa_\beta)^{2^{l+1}-1} \cdot 2^{-\alpha(2^{l+2}-(l+3))} \prod_{i \geq 0} \mathbb{P}(|X_{i,k}| \leq 2^{\alpha i})^{2^{i+l+1}}. \quad (44)$$

Moreover, using (B6), for x large enough, we have $\mathbb{P}(|X_{j,k}| \leq x) \sim 1 - 2\kappa_\beta e^{-|x|^\beta} / (\beta x^{\beta-1})$. Then, there exists $l_\beta > 0$ such that for any $i \geq l_\beta$,

$$1 - \frac{1}{4i^2} \leq \left(1 - \frac{2\kappa_\beta e^{-|2^{\alpha i}|^\beta}}{\beta(2^{\alpha i})^{\beta-1}}\right)^{2^{i+l+1}}, \quad (45)$$

as well as

$$\left(1 - \frac{1}{4i^2}\right) \left(1 - \frac{2\kappa_\beta e^{-|2^{\alpha i}|^\beta}}{\beta(2^{\alpha i})^{\beta-1}}\right)^{2^{i+l+1}} \leq \mathbb{P}(|X_{i,k}| \leq 2^{\alpha i})^{2^{i+l+1}}$$

(46)

and

$$\mathbb{P}(|X_{i,k}| \leq 2^{\alpha i})^{2^{i+l}} \leq \left(1 + \frac{1}{4i(i+1)}\right) \left(1 - \frac{2\kappa_\beta e^{-|2^{\alpha i}|^\beta}}{\beta(2^{\alpha i})^{\beta-1}}\right)^{2^{i+l}}.$$

Using (42), this entails

$$c_{l_\beta} \prod_{i \geq l_\beta} \left(1 - \frac{2\kappa_\beta e^{-|2^{\alpha i}|^\beta}}{\beta(2^{\alpha i})^{\beta-1}}\right)^{2^{i+l+1}} \leq \prod_{i \geq l_\beta} \mathbb{P}(|X_{i,k}| \leq 2^{\alpha i})^{2^{i+l+1}}$$

$$\text{and } \prod_{i \geq l_\beta} \mathbb{P}(|X_{i,k}| \leq 2^{\alpha i})^{2^{i+l}} \leq C_{l_\beta} \prod_{i \geq l_\beta} \left(1 - \frac{2\kappa_\beta e^{-|2^{\alpha i}|^\beta}}{\beta(2^{\alpha i})^{\beta-1}}\right)^{2^{i+l}}$$

with $c_{l_\beta} = \prod_{i \geq l_\beta} (1 - 1/(4i^2)) \in (\pi/2, 1)$ and $C_{l_\beta} = \prod_{i \geq l_\beta} (1 + 1/(4i(i+1))) \in (1, 4/\pi)$. We finally obtain

$$c_{l_\beta} k_\beta \prod_{i=0}^{l_\beta-1} \mathbb{P}(|X_{i,k}| \leq 2^{\alpha i})^{2^{i+l+1}} \prod_{i \geq l_\beta} \left(1 - \frac{2\kappa_\beta e^{-|2^{\alpha i}|^\beta}}{\beta(2^{\alpha i})^{\beta-1}}\right)^{2^{i+l+1}} \leq \mathbb{P}(\ell_{0,0}^1 \leq A)$$

$$\text{and } \mathbb{P}(\ell_{0,0}^1 \leq A) \leq C_{l_\beta} K_\beta \prod_{i=0}^{l_\beta-1} \mathbb{P}(|X_{i,k}| \leq 2^{\alpha i})^{2^{i+l}} \prod_{i \geq l_\beta} \left(1 - \frac{2\kappa_\beta e^{-|2^{\alpha i}|^\beta}}{\beta(2^{\alpha i})^{\beta-1}}\right)^{2^{i+l}} \quad (47)$$

with $k_\beta = (2\kappa_\beta)^{2^{l+1}-1} \cdot 2^{-\alpha(2^{l+2}-(l+3))}$ and $K_\beta = (2\kappa_\beta)^{2^{l-1}} \cdot 2^{-\alpha(2^{l+1}-(l+2))}$ come from (43) and (44). Note that for $\tau \in \{0, 1\}$, by (45), there exists $\Lambda_\beta \in (1, \pi/2)$ such that

$$\prod_{i \geq l_\beta} \left(1 - \frac{2\kappa_\beta e^{-|2^{\alpha i}|^\beta}}{\beta(2^{\alpha i})^{\beta-1}}\right)^{2^{i+l+\tau}} = \left[\Lambda_\beta \prod_{i \geq l_\beta} \left(1 - \frac{1}{4i^2}\right)\right]^{2^{l+\tau}} = (c_{l_\beta} \Lambda_\beta)^{2^{l+\tau}} > 0, \quad (48)$$

so that the infinite products appearing on the left and right sides of (47) are equal to strictly positive constants. Inserting the previous results into (43) and (44), we find that

$$\lambda_1 2^{\alpha(l+3)} \left(\frac{2c_{l_\beta} \kappa_\beta \Lambda_\beta}{2^{2\alpha}}\right)^{2^{l+1}} \leq \mathbb{P}(\ell_{0,0}^1 \leq A) \leq \min \left\{ \lambda_2 2^{\alpha(l+2)} \left(\frac{2c_{l_\beta} \kappa_\beta \Lambda_\beta}{2^{2\alpha}}\right)^{2^l}; 1 \right\},$$

where λ_1 and λ_2 are positive constants proportional to

$$\lambda_1 = (2\kappa_\beta)^{-1} k_1 c_{l_\beta} \prod_{i=0}^{l_\beta-1} \mathbb{P}(|X_{i,k}| \leq 2^{\alpha i})^{2^{i+l+1}} \quad \text{and} \quad \lambda_2 = (2\kappa_\beta)^{-1} k_2 c_{l_\beta} \prod_{i=0}^{l_\beta-1} \mathbb{P}(|X_{i,k}| \leq 2^{\alpha i})^{2^{i+l}}$$

Noting by (40) that $2c_{l_\beta} \kappa_\beta \Lambda_\beta / 2^{2\alpha} < 1$,

$$\lambda_1 \frac{2^\alpha}{A} \exp\left(A^{-1/\alpha} \log\left(\frac{2c_{l_\beta} \kappa_\beta \Lambda_\beta}{2^{2\alpha}}\right)\right) \leq \mathbb{P}(\ell_{0,0}^1 \leq A) \leq \lambda_2 \frac{2^\alpha}{A} \exp\left(A^{-1/\alpha} \log\left(\frac{2c_{l_\beta} \kappa_\beta \Lambda_\beta}{2^{2\alpha}}\right)\right),$$

as $A \in (2^{-\alpha(l+1)}, 2^{-\alpha l}]$. Hence the result.

Distribution of large leaders Let $\beta \in \mathbb{R}_+^*$. We are interested in the behaviour of large log-leaders, i.e. we aim at approximating $\mathbb{P}(\ell_{0,0}^1 > A)$ for $A > 0$ sufficiently large. First,

$$\begin{aligned} \mathbb{P}(\ell_{0,0}^1 > A) &= \mathbb{P}\left(\sup_{\lambda \subset I} |c_\lambda| > A\right) \\ &\leq \sum_{\lambda \subset I} \mathbb{P}(|c_\lambda| > A) \\ &= \sum_{(j,k): \lambda \subset I} \mathbb{P}(|c_{j,k}| > A) \\ &= \sum_{(j,k): \lambda \subset I} \mathbb{P}(|X_{j,k}| > 2^{\alpha j} A) \\ &= \sum_{j \in \mathbb{N}} 2^j \mathbb{P}(|X_{j,k}| > 2^{\alpha j} A), \end{aligned} \quad (49)$$

where we have used that the $X_{j,k}$ are identically distributed in the last line. Let A be sufficiently large, meaning any $A > A_\beta$, where $A_\beta > 0$ is chosen such that $0.99\kappa_\beta \frac{e^{-A_\beta}}{\beta A_\beta^{\beta-1}} \leq \mathbb{P}(X_{0,k} > A_\beta) \leq 1.01\kappa_\beta \frac{e^{-A_\beta}}{\beta A_\beta^{\beta-1}}$ (see (B1)). Then, for all $j \in \mathbb{N}$,

$$0.99 \cdot 2^j \left(\frac{\kappa_\beta e^{-(2^{\alpha j} A)^\beta}}{\beta(2^{\alpha j} A)^{\beta-1}}\right) \leq 2^j \mathbb{P}(|X_{j,k}| > 2^{\alpha j} A) \leq 1.01 \cdot 2^j \left(\frac{\kappa_\beta e^{-(2^{\alpha j} A)^\beta}}{\beta(2^{\alpha j} A)^{\beta-1}}\right). \quad (50)$$

Note that (see Remark 3), since $2^{\alpha\beta}(1/\log(2) - \alpha\beta + \log_2(\alpha\beta \log(2))) - 1 > 0$, it follows that for any $j \geq 0$, $e^{-(2^{\alpha j} A)^\beta} \leq e^{-A^\beta} e^{-j(2^{\alpha j} A)^\beta}$. Combining this with (49) and (50) entails

$$\mathbb{P}(\ell_{0,0}^1 > A) \leq \frac{1.01\kappa_\beta e^{-A^\beta}}{\beta A^{\beta-1}} \sum_{j \geq 0} \frac{e^{-j(2^{\alpha j} A)^\beta} \cdot 2^j}{2^{\alpha(\beta-1)j}} \leq \frac{1.01\kappa_\beta e^{-A^\beta}}{\beta A^{\beta-1}} \frac{1}{1 - \frac{2^{1-\alpha(\beta-1)}}{e^{2^{\alpha\beta} A^\beta}}}. \quad (51)$$

It is then enough to determine A_β according to the values of $\beta \in (0, 1)$.

Case 1: $\beta > 1$. Using (B3), we can choose A_β such that

$$0.99 = \frac{1}{1 + (\beta - 1)/(\beta A_\beta^\beta)},$$

which enables us to satisfy (50) for $j = 0$. We can check that (50) holds for any $A > A_\beta$ and for all $j \in \mathbb{N}$.

Case 2: $0 < \beta < 1$. Using (B4), we can choose A_β such that

$$\frac{1}{1 - (1 - \beta)/(\beta A_\beta^\beta)} = 1.01,$$

which is (50) for $j = 0$. As before, we can check that (50) holds for any $A > A_\beta$ and for all $j \in \mathbb{N}$.

Case 3: $\beta = 1$. In that case, using that $\mathbb{P}(|X_{j,k}| > 2^{\alpha j} A) = e^{-2^{\alpha j} A}$, we get by (49) that

$$\begin{aligned} \mathbb{P}(\ell_{0,0}^1 > A) &\leq \sum_{j \in \mathbb{N}} 2^j e^{-2^{\alpha j} A} \\ &\leq e^{-A} \sum_{j \in \mathbb{N}} 2^j e^{-j 2^{\alpha} A} = e^{-A} \frac{1}{1 - \frac{2}{e^{2^{\alpha} A}}}, \end{aligned}$$

using that we have chosen α (see Remark 3) such that $2^{\alpha j} A \geq A(1 + 2^{\alpha} j)$ for all $j \in \mathbb{N}$. \square

Example 1 Let us choose $\beta = 2$. Then, the $X_{j,k}$ are Gaussian random variables with variance $1/2$ and $\kappa_\beta = 1/\sqrt{\pi}$.

Distribution of small leaders To obtain an expression of (38) with explicit values, we need to choose α . For example, let $\alpha = 1$, and $l_2 = 3$, so that $0.99 e^{-x^2} / (2\sqrt{\pi}x) \leq \mathbb{P}(X > x) \leq e^{-x^2} / (2\sqrt{\pi}x)$ for all $x \geq 2^{l_2}$. Using (43) as well as $c_{l_2} = \prod_{j \geq 3} (1 - 1/(4j^2)) = 128/(45\pi)$, we obtain that and

$$\mathbb{P}(\ell_{0,0}^1 \leq A) = \Theta \left(2A^{-1} \exp \left(A^{-1} \left(\log \left(\frac{2c_{l_2} \Lambda_2}{\sqrt{\pi}} \right) \right) - 2 \log(2) \right) \right). \quad (52)$$

where $c_{l_2} \Lambda_2 \in (256/(45\pi^2), 1)$. We can check that $2c_{l_2} \Lambda_2 / \sqrt{\pi} - 2 \log(2) < 2/\sqrt{\pi} - 2 \log 2 < 0$.

Distribution of large leaders we can choose A_2 such that

$$0.99 = \frac{1}{1 + 1/(2A_2^2)} \text{ i.e. } A_2 = \sqrt{99/2} \simeq 7.04.$$

Then for all $A > A_2$, by (39), there exists $c > 0$ such that

$$\mathbb{P}(\ell_{0,0}^1 > A) \leq \frac{c e^{-A^2}}{A} \frac{1}{1 - \frac{2^{1-\alpha}}{e^{2^{\alpha} A^2}}}. \quad (53)$$

Remark 5 Both results (52) and (53) align with the negative outcomes of the log-normality test performed on the leaders (see Section 3.1): even when the distribution of the variables $X_{j,k}$ is Gaussian, the tails of the distribution of the log-leaders are significantly lighter than those of a Gaussian.

6 Conclusion and prospects

In this work, we focused on the distribution of log-leaders, key quantities for estimating the multifractal spectrum. The first step involved rejecting the commonly held assumption that log-leaders follow Gaussian distributions. A normality test was applied to the log-leaders of various types of processes (fractional Brownian motion, compound Poisson process, multifractal random walk) as well as to heart rate and speed data from marathon runners. We then applied an experimentally validated test for log-concavity, which allowed us to propose a wider nonparametric model for log-leaders: log-concave distributions. This allows for a reassessment of the estimation of the parameters c_1 and c_2 and for establishing a confidence interval for the estimation of c_1 based on the CLT, without relying on the Gaussianity assumption. Finally, we conducted a preliminary theoretical study which allowed us to approximate the cumulative distribution function of the log-leaders for random wavelet series, assuming independence of wavelet coefficients both within and across scales. This corroborates the empirical discovery that, although the distributions of log-leaders are not normal, they belong to the larger class of log-concave distributions. This exploratory work should help refine the methods used in multifractal analysis until now, which seem numerically justified but whose validity is demonstrated under the overly restrictive/invalidated assumption of normality.

A primary direction for applying and extending this work is in estimating the scaling exponents that characterize scale invariance properties, as well as constructing confidence intervals to measure their quality. Standard methods for constructing such bounds are often based on Gaussian theory; they prove effective for Gaussian self-similar processes [78, 79] but perform poorly when applied to multifractal processes due to their non-Gaussian nature. However, the use of nonparametric or Empirical Cumulative Distribution Function bootstrap (ECDF-bootstrap) allows for circumventing the problem by assuming that little to nothing is known about the underlying model of the data (see [14]). To take advantage of the fact that the distributions of the log-leaders are log-concave, it would be interesting to explore other types of methods, such as those studied by Azadbakhsh, Jankowski and Gao [80], for computing confidence intervals for log-concave densities. These methods are notably based on the fact that the log-concave MLE can be used in Monte Carlo bootstrap procedures, as noted by Cule and Samworth [69]. We have provided a confidence interval for c_1 based on the CLT. Establishing one for c_2 would require computing a confidence interval for the variance of log-concave distributions—a challenging problem that remains unsolved. Furthermore, our result nuances that of [38], which state that the distribution of the log-leaders can be approximated by a Gaussian. Based on this assumption, Combexelle, Wendt, Dobigeon, Tourneret, McLaughlin, and Abry construct a semi-parametric model for the statistics of the logarithm, which they then use to define and study a Bayesian estimator of the multifractality parameter for synthetic multifractal processes in [38], image texture [16] and multivariate time series in [17]. From this perspective, it would be interesting to extend or adapt the semi-parametric model and Bayesian procedure they introduced by considering that the distributions of the log-leaders are log-concave rather than assuming that they can be approximated by a Gaussian random variable.

Note also that, in the present article, we only considered the two major multifractality parameters used for classification which are deduced from wavelet leaders, i.e. c_1 and c_2 . The third major multifractality parameter, namely, the uniform regularity exponent H_f^{\min} , is derived directly from wavelet coefficients; its statistical estimation will be addressed in [19].

Finally, it would be valuable to relax the assumption of independence between scale coefficients, as used in the theoretical study of Section 5, and to develop a model that addresses the dependencies highlighted numerically (see for instance [21]). A first question is to determine which results concerning the multifractal analysis of random wavelet series may be modified if one drops the assumption of independence between scale; this is one of the topics addressed in the forthcoming paper [19], where we will focus on the important example where the laws of wavelet coefficients are Gaussian mixtures.

Another important issue is to extend this analysis to p -leaders, for which the supremum of wavelet coefficients in the definition of wavelet leaders is replaced by a l^p -norm. Indeed the use of p -leaders has a wider range of validity (leaders require a uniform regularity assumption which is often not met in practice, see [25]) and furthermore, it has been noticed that a multifractal analysis based on p -leaders for p close to 2 enjoys better statistical properties than when using wavelet leaders [27, 81].

Acknowledgements. The authors are very grateful to Véronique Billat from the IBISC laboratory at Université d'Évry Paris-Saclay for allowing them to use the marathon runners data which she and her team collected.

Appendix A Equality between the 1-leader and the 3-leader scaling functions

Proof of Proposition 3 For simplicity, we prove the result in the one-variable case, noting that it extends naturally to the general case. First, since for all $\lambda \geq 0$, $\ell_\lambda^1 \leq \ell_\lambda^3$, it follows that all $q > 0$ and j , $S_1(j, q) \leq S_3(j, q)$, so that

$$\forall q > 0, \quad \zeta_1(q) \geq \zeta_3(q).$$

Similarly, we have that for all $q < 0$ and j , $S_1(j, q) \geq S_3(j, q)$ so that

$$\forall q < 0, \quad \zeta_1(q) \leq \zeta_3(q).$$

In order to obtain the reversed inequalities, we note that $\ell_\lambda^3 = \max(\ell_{\lambda^-}^1, \ell_\lambda^1, \ell_{\lambda^+}^1)$, where λ^- and λ^+ are the two dyadic intervals neighbours to λ and of the same generation. It follows that for all $q > 0$, $S_3(j, q) \leq 3S_1(j, q)$, so that

$$\forall q > 0, \quad \zeta_3(q) \geq \zeta_1(q).$$

Assume now that $q < 0$. We denote by $\lambda'(\lambda)$ and $\lambda''(\lambda)$ the two sub-intervals of λ of generation $j+2$ which are included in the interior of λ ($\lambda'(\lambda)$ being on the left of $\lambda''(\lambda)$). It follows that $3\lambda'(\lambda) \subset \lambda$, so that

$$\ell_{\lambda'(\lambda)}^3 = \sup_{\lambda'' \subset 3\lambda'(\lambda)} |c_{\lambda''}| \leq \sup_{\lambda'' \subset \lambda} |c_{\lambda''}| = \ell_\lambda^1.$$

Denote by Λ_j the set of dyadic intervals of generation j (i.e. of length 2^{-j}). It follows that

$$\forall q < 0, \quad \sum_{\lambda \in \Lambda_j} |\ell_\lambda^1|^q \leq \sum_{\lambda \in \Lambda_j} |\ell_{\lambda'(\lambda)}^3|^q \leq \sum_{\lambda' \in \Lambda_{j+2}} |\ell_{\lambda'}^3|^q.$$

It follows that

$$\forall q < 0, \quad S_1(j, q) \leq 4 \cdot S_3(j + 2, q),$$

so that

$$\forall q < 0, \quad \zeta_1(q) \geq \zeta_3(q).$$

Putting together the four inequalities we have proved between values of the scaling functions yields (35). \square

Appendix B General bounds on Mills ratio

In probability theory, the Mills ratio [82] states that for a continuous real random variable X with density f and for any $x \in \mathbb{R}$,

$$\frac{I(x)}{f(x)} = \lim_{\varepsilon \rightarrow 0} \frac{1}{\varepsilon} \mathbb{P}(x < X \leq x + \varepsilon | X > x), \quad (\text{B1})$$

where for all $x \in \mathbb{R}$, we define $I(x) = \mathbb{P}(X > x)$. Bounding (B1) provides insights on the distribution of the tails of a random variable. For instance, if X has a standard normal distribution, for all $x > 0$,

$$\frac{x e^{-x^2/2}}{\sqrt{2\pi}(x^2 + 1)} \leq I(x) \leq \frac{e^{-x^2/2}}{\sqrt{2\pi}x}.$$

In the same spirit, in the following lemma, we provide bounds for random variables having an exponential density.

Lemma 1 (General bounds for Mills ratio) Let $g : \mathbb{R} \rightarrow \mathbb{R}$ be a twice differentiable positive function such that g' is positive on \mathbb{R}_+^* and g'' has a constant sign on \mathbb{R}_+ . Assume, moreover, that there exists a function $M : \mathbb{R}_+ \rightarrow \mathbb{R}_+$ such that for $x > 0$,

$$\sup_{t \in [x, \infty)} \left| \frac{g''(t)}{(g'(t))^2} \right| \leq M(x).$$

Let X be a real random variable with density $f = \kappa e^{-g}$, where $\kappa > 0$ is a normalisation constant. For all $x \in \mathbb{R}$, we define $I(x) = \mathbb{P}(X > x) = \int_x^\infty \kappa e^{-g(t)} dt$. Then,

$$\forall x \in \mathbb{R}_+^*, \quad \frac{f(x)}{g'(x)(1 + M(x)\mathbf{1}_{\{g'' > 0\}})} \leq I(x) \leq \frac{f(x)}{g'(x)(1 - M(x)\mathbf{1}_{\{g'' < 0\}})}. \quad (\text{B2})$$

Proof For $x \in \mathbb{R}_+^*$,

$$\begin{aligned} \kappa^{-1} I(x) &= \int_x^\infty \frac{g'(t)}{g'(t)} e^{-g(t)} dt = \lim_{A \rightarrow \infty} \left[-\frac{1}{g'(t)} e^{-g(t)} \right]_x^A - \int_x^\infty \frac{g''(t)}{(g'(t))^2} e^{-g(t)} dt \\ &= \frac{1}{g'(x)} e^{-g(x)} - \int_x^\infty \frac{g''(t)}{(g'(t))^2} e^{-g(t)} dt. \end{aligned}$$

If $g'' > 0$, we get that for any $x \in \mathbb{R}_+^*$,

$$\frac{e^{-g(x)}}{g'(x)} - \kappa^{-1} M(x) I(x) \leq \kappa^{-1} I(x) \leq \frac{e^{-g(x)}}{g'(x)},$$

whereas if $g'' < 0$,

$$\frac{e^{-g(x)}}{g'(x)} \leq \kappa^{-1} I(x) \leq \frac{e^{-g(x)}}{g'(x)} + \kappa^{-1} m(x) I(x).$$

The two inequalities lead to (B2). \square

Example 2 1. Standard Gaussian. Taking $g(x) = x^2/2$ and $\kappa = (2\pi)^{-1/2}$, we find $M(x) = 1/x^2$. This boils down to the well-known result:

$$\forall x > 0, \quad \frac{1}{\sqrt{2\pi}} \frac{e^{-x^2/2}}{x(1+1/x^2)} \leq I(x) \leq \frac{1}{\sqrt{2\pi}} \frac{e^{-x^2/2}}{x}.$$

2. **Generalized Gaussian with light tails** ($\beta > 1$). Taking $g(x) = |x|^\beta$ and $\kappa_\beta = \beta/(2\Gamma(1/\beta))$ with $\beta > 1$, clearly $g' > 0$ and $g'' > 0$ on \mathbb{R}_+^* . We have that for all $x > 0$, $M(x) = (\beta - 1)/(\beta x^\beta)$ and

$$\frac{1}{2\Gamma(1/\beta)} \frac{e^{-x^\beta}}{x^{\beta-1}(1+(\beta-1)/(\beta x^\beta))} \leq I(x) \leq \frac{1}{2\Gamma(1/\beta)} \frac{e^{-x^\beta}}{x^{\beta-1}}. \quad (\text{B3})$$

3. **Generalized Gaussian with heavy tails** ($0 < \beta < 1$). Taking $g(x) = |x|^\beta$ and $\kappa = \beta/(2\Gamma(1/\beta))$ with $\beta < 1$, we check that $g' > 0$ and $g'' < 0$ on \mathbb{R}_+^* . We have that for all $x > 0$, $M(x) = (1 - \beta)/(\beta x^\beta)$ and that

$$\frac{x^{1-\beta} e^{-x^\beta}}{2\Gamma(1/\beta)} \leq I(x) \leq \frac{1}{2\Gamma(1/\beta)} \frac{x^{1-\beta} e^{-x^\beta}}{(1 - (1 - \beta)/(\beta x^\beta))}. \quad (\text{B4})$$

4. **Laplace distribution** ($\beta = 1$). Taking $g(x) = |x|$ and $\kappa = 1/(2\Gamma(1)) = 1/2$ and

$$\forall x > 0, \quad I(x) = \frac{1}{2} e^{-x} =: f_1(x). \quad (\text{B5})$$

5. **Asymptotics.** Given the density (33) of a generalized Gaussian random variable X , we have, asymptotically,

$$\mathbb{P}(X > x) \underset{x \rightarrow \infty}{\sim} \frac{f_\beta(x)}{\beta x^{\beta-1}}. \quad (\text{B6})$$

Note that, since X is symmetric, we obtain, asymptotically,

$$\mathbb{P}(|X| \leq x) = 1 - 2\mathbb{P}(X > x) \underset{x}{\sim} 1 - \frac{2f_\beta(x)}{\beta x^{\beta-1}}.$$

References

- [1] Cohen, S., Istas, J.: Fractional Fields and Applications. Mathematics and applications, vol. 2. Springer, Berlin Heidelberg New York (2013)

- [2] Ayache, A.: *Multifractional Stochastic Fields: Wavelet Strategies in Multifractional Frameworks*. World Scientific, ??? (2018)
- [3] Istas, J., Lang, G.: Quadratic variations and estimation of the local Hölder index of a Gaussian process. In: *Annales de l'Institut Henri Poincaré (B) Probability and Statistics*, vol. 33, pp. 407–436 (1997). Elsevier
- [4] Bertrand, P.R., Fhima, M., Guillin, A.: Local estimation of the hurst index of multifractional brownian motion by increment ratio statistic method. *ESAIM: probability and statistics* **17**, 307–327 (2013)
- [5] Ayache, A., Hamonier, J.: Linear fractional stable motion: A wavelet estimator of the α parameter. *Statistics & Probability Letters* **82**(8), 1569–1575 (2012)
- [6] Ayache, A., Hamonier, J.: Linear multifractional stable motion: wavelet estimation of $h(\cdot)$ and α parameters. *Lithuanian Mathematical Journal* **55**, 159–192 (2015)
- [7] Jin, S., Peng, Q., Schellhorn, H.: Estimation of the pointwise Hölder exponent of hidden multifractional Brownian motion using wavelet coefficients. *Statistical Inference for Stochastic Processes* **21**, 113–140 (2018)
- [8] Parisi, G., Frisch, U.: Fully developed turbulence and intermittency. In: Ghil, M., Benzi, R., Parisi, G. (eds.) *Turbulence and Predictability in Geophysical Fluid Dynamics and Climate Dynamics*. Proc. of Int. School, p. 84. North-Holland, Amsterdam (1985)
- [9] Kolmogorov, A.N.: a) dissipation of energy in the locally isotropic turbulence. b) the local structure of turbulence in incompressible viscous fluid for very large Reynolds number. c) on degeneration of isotropic turbulence in an incompressible viscous liquid. In: Friedlander, S.K., Topper, L. (eds.) *Turbulence, Classic Papers on Statistical Theory*, pp. 151–161. Interscience publishers, ??? (1941)
- [10] Muzy, J.-F., Bacry, E., Arneodo, A.: Wavelets and multifractal formalism for singular signals: Application to turbulence data. *Physical review letters* **67**(25), 3515 (1991)
- [11] Kantelhardt, J., Koscielny-Bunde, E., Rego, H., Havlin, S., Bunde, A.: Detecting long-range correlations with detrended fluctuation analysis. *Physica A: Statistical Mechanics and its Applications* **295**(3-4), 441–454 (2001)
- [12] Lashermes, B., Roux, S.G., Abry, P., Jaffard, S.: Comprehensive multifractal analysis of turbulent velocity using the wavelet leaders. *European Physical Journal B* **61**(2), 201–215 (2008)
- [13] Wendt, H., Abry, P.: Multifractality tests using bootstrapped wavelet leaders. *IEEE T. Signal Proces.* **55**(10), 4811–4820 (2007)

- [14] Wendt, H., Abry, P., Jaffard, S.: Bootstrap for empirical multifractal analysis. *IEEE signal processing magazine* **24**(4), 38–48 (2007)
- [15] Wendt, H., Roux, S.G., Jaffard, S., Abry, P.: Wavelet leaders and bootstrap for multifractal analysis of images. *Signal Processing* **89**(6), 1100–1114 (2009)
- [16] Combrexelle, S., Wendt, H., Dobigeon, N., Tourneret, J.-Y., McLaughlin, S., Abry, P.: Bayesian estimation of the multifractality parameter for image texture using a Whittle approximation. *IEEE Transactions on Image Processing* **24**(8), 2540–2551 (2015)
- [17] Combrexelle, S., Wendt, H., Altmann, Y., Tourneret, J.-Y., McLaughlin, S., Abry, P.: Bayesian estimation for the local assessment of the multifractality parameter of multivariate time series. In: *Proc. European Signal Processing Conference (EUSIPCO)*, Budapest, Hunagry (2016)
- [18] Leon, L., Wendt, H., Tourneret, J.-Y., Abry, P.: A bayesian framework for multivariate multifractal analysis. *IEEE T. Signal Proces.* **70**, 3663–3675 (2022)
- [19] W. Ben Nasr, H.H., Jaffard, S.: Multifractal analysis of random wavelet series with generalized gaussian mixture statistics. In preparation (2025)
- [20] Cule, M., Samworth, R., Stewart, M.: Maximum likelihood estimation of a multi-dimensional log-concave density. *Journal of the Royal Statistical Society Series B: Statistical Methodology* **72**(5), 545–607 (2010)
- [21] Morel, R., Rochette, G., Leonarduzzi, R., Bouchaud, J.-P., Mallat, S.: Scale dependencies and self-similar models with wavelet scattering spectra. *Applied and Computational Harmonic Analysis* **75**, 101724 (2025)
- [22] Meyer, Y.: *Wavelets and Operators* vol. 37. Cambridge university press, ??? (1992)
- [23] Daubechies, I.: Orthonormal bases of compactly supported wavelets. *Comm. Pure and App. Math.* **41**, 909–996 (1988)
- [24] Jaffard, S.: Wavelet techniques in multifractal analysis. In: Lapidus, M., Franchini, M. (eds.) *Fractal Geometry and Applications: A Jubilee of Benoît Mandelbrot*, *Proc. Symp. Pure Math.*, vol. 72(2), pp. 91–152. AMS, ??? (2004)
- [25] Jaffard, S., Abry, P., Wendt, H.: In: Frame, M., Cohen, N. (eds.) *Irregularities and Scaling in Signal and Image Processing: Multifractal Analysis*, pp. 31–116. World scientific publishing, Singapore (2015)
- [26] Jaffard, S., Lashermes, B., Abry, P.: Wavelet leaders in multifractal analysis. In: *Wavelet Analysis and Applications*, pp. 201–246 (2007). Springer
- [27] Leonarduzzi, R., Wendt, H., Roux, S.G., Torres, M.E., Melot, C., Jaffard, S.,

- Abry, P.: p-exponent and p-leaders, Part II: Multifractal analysis. Relations to Detrended Fluctuation Analysis. *Physica A: Statistical Mechanics and its Applications* **448**, 319–339 (2016)
- [28] Portilla, J., Strela, V., Wainwright, M., Simoncelli, E.: Adaptive Wiener denoising using a Gaussian scale mixture model in the wavelet domain. In: *Proceedings 2001 International Conference on Image Processing (Cat. No. 01CH37205)*, vol. 2, pp. 37–40 (2001). IEEE
- [29] Lyu, S., Simoncelli, E.: Modeling multiscale subbands of photographic images with fields of Gaussian scale mixtures. *IEEE Transactions on pattern analysis and machine intelligence* **31**(4), 693–706 (2008)
- [30] Jaffard, S.: Beyond Besov spaces, part 2: Oscillation spaces. *Constructive Approximation* **21**(1), 29–61 (2005) <https://doi.org/10.1007/s00365-004-0558-5>
- [31] Lashermes, B., Roux, G., Abry, P., Jaffard, S.: Comprehensive multifractal analysis of turbulent velocity using the wavelet leaders. *The European Physical Journal B* **61**, 201–215 (2008)
- [32] Castaing, B., Gagne, Y., Marchand, M.: Log-similarity for turbulent flows? *Physica D: Nonlinear Phenomena* **68**(3), 387–400 (1993) [https://doi.org/10.1016/0167-2789\(93\)90132-K](https://doi.org/10.1016/0167-2789(93)90132-K)
- [33] Delour, J., Muzy, J.-F., Arneodo, A.: Intermittency of 1d velocity spatial profiles in turbulence: a magnitude cumulant analysis. *The European Physical Journal B* **23**, 243–248 (2001)
- [34] Wendt, H.: Contributions of wavelet leaders and bootstrap to multifractal analysis: Images, estimation performance, dependence structure and vanishing moments. confidence intervals and hypothesis tests. PhD thesis, Ecole Normale Supérieure de Lyon (2008)
- [35] Wendt, H., Roux, S.-G., Abry, P.: Bootstrap for log wavelet leaders cumulant based multifractal analysis. In: *2006 14th European Signal Processing Conference*, pp. 1–5 (2006). IEEE
- [36] Ciuciu, P., Abry, P., Rabrait, C., Wendt, H.: Log wavelet leaders cumulant based multifractal analysis of evi fmri time series: evidence of scaling in ongoing and evoked brain activity. *IEEE J. of Selected Topics in Signal Proces.* **2**(6), 929–943 (2009)
- [37] Combrexelle, S.: Multifractal analysis for multivariate data with application to remote sensing. PhD thesis, Institut National Polytechnique de Toulouse-INPT; Heriot-Watt University (2016)
- [38] Wendt, H., Dobigeon, N., Tourneret, J.-Y., Abry, P.: Bayesian estimation for the

- multifractality parameter. In: 2013 IEEE International Conference on Acoustics, Speech and Signal Processing, pp. 6556–6560 (2013). IEEE
- [39] Flandrin, P.: Wavelet analysis and synthesis of fractional brownian motion. *IEEE Transactions on information theory* **38**(2), 910–917 (1992)
- [40] Hurteaux, Y.: An introduction to mandelbrot cascades. *New Trends in Applied Harmonic Analysis: Sparse Representations, Compressed Sensing, and Multifractal Analysis*, 67–105 (2016)
- [41] Mandelbrot, B.: Intermittent turbulence in self-similar cascades: divergence of high moments and dimension of the carrier. *Multifractals and 1/f Noise: Wild Self-Affinity in Physics (1963–1976)*, 317–357 (1999)
- [42] Barral, J.: Continuity of the multifractal spectrum of a random statistically self-similar measure. *Journal of Theoretical Probability* **13**(4), 1027–1060 (2000)
- [43] Barral, J., Mandelbrot, B.: Multifractal products of cylindrical pulses. *Probability Theory and Related Fields* **124**(3), 409–430 (2002)
- [44] Chainais, P., Riedi, R., Abry, P.: Compound Poisson cascades. In: *Colloque Autosimilarité et Applications* (2002). Clermont-Ferrand
- [45] Chainais, P.: Infinitely divisible cascades to model the statistics of natural images. *IEEE Transactions on Pattern Analysis and Machine Intelligence* **29**(12), 2105–2119 (2007)
- [46] Frezza, D., Thompson, J., Slater, D., Jacyna, G.: Simulating multifractal signals for risk assessment. In: 2019 Winter Simulation Conference (WSC), pp. 536–547 (2019). IEEE
- [47] Bacry, E., Delour, J., Muzy, J.F.: Multifractal random walk. *Physical review E* **64**(2), 026103 (2001)
- [48] Abry, P., Chainais, P., Coutin, L., Pipiras, V.: Multifractal random walks as fractional wiener integrals. *IEEE Transactions on Information Theory* **55**(8), 3825–3846 (2009)
- [49] Wesfreid, E., Billat, V., Meyer, Y.: Multifractal analysis of heartbeat time series in human races. *Appl. Comput. Harmon. Anal.* (2010)
- [50] Billat, V., Mille-Hamard, L., Meyer, Y., Wesfreid, E.: Detection of changes in the fractal scaling of heart rate and speed in a marathon race. *Physica A: Statistical Mechanics and its Applications* **388**(18), 3798–3808 (2009)
- [51] Jaffard, S., Saës, G., Ben Nasr, W., Palacin, F., Billat, V.: A review of univariate and multivariate multifractal analysis illustrated by the analysis of marathon

- runners physiological data. In: *Mathematical Analysis and Applications - Plenary Lectures - ISAAC 2021*, Springer Proceedings in Mathematics and Statistics (2023)
- [52] Abry, P., Wendt, H., Jaffard, S., Helgason, H., Gonçalves, P., Pereira, E., G., C., Gaucherand, P., Doret, M.: Methodology for multifractal analysis of heart rate variability: From lf/hf ratio to wavelet leaders. In: *2010 Annual International Conference of the IEEE Engineering in Medicine and Biology*, pp. 106–109 (2010). IEEE
- [53] Mendes, M., Pala, A.: Type I error rate and power of three normality tests. *Pakistan Journal of Information and Technology* **2**(2), 135–139 (2003)
- [54] Keskin, S.: Comparison of several univariate normality tests regarding type i error rate and power of the test in simulation based small samples. *Journal of Applied Science Research* **2**(5), 296–300 (2006)
- [55] Mohd Razali, N., Yap, B.: Power comparisons of Shapiro-Wilk, Kolmogorov-Smirnov, Lilliefors and Anderson-Darling tests. *J. Stat. Model. Analytics* **2**, 21–33 (2011)
- [56] Althouse, L.A., Ware, W., Ferron, J.: Detecting departures from normality: A Monte-Carlo simulation of a new omnibus test based on moments. (1998)
- [57] Royston, P.: An extension of Shapiro and Wilk’s W test for normality to large samples. *Journal of the Royal Statistical Society: Series C (Applied Statistics)* **31**(2), 115–124 (1982)
- [58] Royston, P.: Algorithm as 177: Expected normal order statistics (exact and approximate). *Journal of the royal statistical society. Series C (Applied statistics)* **31**(2), 161–165 (1982)
- [59] Royston, P.: Remark as r94: A remark on algorithm as 181: The w-test for normality. *Journal of the Royal Statistical Society. Series C (Applied Statistics)* **44**(4), 547–551 (1995)
- [60] Ibragimov, I.A.: On the composition of unimodal distributions. *Theory of Probability & Its Applications* **1**(2), 255–260 (1956)
- [61] Walther, G.: Inference and modeling with log-concave distributions. *Statistical Science*, 319–327 (2009)
- [62] Mandelbrot, B.: *The Variation of Certain Speculative Prices*. Springer, ??? (1997)
- [63] Van Tran, Q., Kukal, J.: A novel heavy tail distribution of logarithmic returns of cryptocurrencies. *Finance Research Letters* **47**, 102574 (2022)
- [64] Resnick, S.I.: *Heavy-tail Phenomena: Probabilistic and Statistical Modeling* vol.

- 10, Springer Science and Business Media, (2007)
- [65] Badía, F.G., Sangüesa, C., Federgruen, A.: Log-concavity of compound distributions with applications in operational and actuarial models. *Probability in the Engineering and Informational Sciences* **35**(2), 210–235 (2021)
 - [66] Nandal, A., Dhaka, A., Gamboa-Rosales, H.i., Marina, N., Galvan-Tejada, J., Galvan-Tejada, C., Moreno-Baez, A., Celaya-Padilla, J., Luna-Garcia, H.: Sensitivity and variability analysis for image denoising using maximum likelihood estimation of exponential distribution. *Circuits, Systems, and Signal Processing* **37**, 3903–3926 (2018)
 - [67] Sengupta, D., Nanda, A.: Log-concave and concave distributions in reliability. *Naval Research Logistics (NRL)* **46**(4), 419–433 (1999)
 - [68] Bagnoli, M., Bergstrom, T.: Log-concave probability and its applications. In: *Rationality and Equilibrium: A Symposium in Honor of Marcel K. Richter*, pp. 217–241 (2006). Springer
 - [69] Cule, M., Samworth, R.: Theoretical properties of the log-concave maximum likelihood estimator of a multidimensional density. *Electronic Journal of Statistics* **4**, 254–270 (2010) <https://doi.org/10.1214/09-EJS505>
 - [70] Jacyna, G., Frezza, D., Slater, D., Thompson, J.: An improved model of wavelet leader covariance for estimating multifractal properties. *ACM Transactions on Modeling and Computer Simulation* **34**(1), 1–22 (2023)
 - [71] Shevtsova, I.: On the absolute constants in the Berry-Esseen-type inequalities. In: *Doklady Mathematics*, vol. 89 (2014)
 - [72] Wendt, H., Abry, P.: Bootstrap for multifractal analysis. In: *2006 IEEE International Conference on Acoustics Speech and Signal Processing Proceedings*, vol. 3, p. (2006). IEEE
 - [73] Aubry, J.M., Jaffard, S.: Random wavelet series. *Communications In Mathematical Physics* **227**(3), 483–514 (2002)
 - [74] Wainwright, M., Simoncelli, E., Willsky, A.: Random cascades on wavelet trees and their use in analyzing and modeling natural images. *Applied and Computational Harmonic Analysis* **11**(1), 89–123 (2001)
 - [75] Chipman, H., Kolaczyk, E., McCulloch, R.: Adaptive Bayesian wavelet shrinkage. *Journal of the American Statistical Association*, 1413–1421 (1997)
 - [76] Abramovich, F., Sapatinas, T., Silverman, B.: Wavelet thresholding via a Bayesian approach. *Journal of the Royal Statistical Society: Series B (Statistical Methodology)* **60**(4), 725–749 (1998)

- [77] Strela, V., Portilla, J., Simoncelli, E.: Image denoising using a local Gaussian scale mixture model in the wavelet domain. In: *Wavelet Applications in Signal and Image Processing VIII*, vol. 4119, pp. 363–371 (2000). SPIE
- [78] Abry, P., Flandrin, P., Taqqu, M.S., Veitch, D.: Wavelets for the analysis, estimation, and synthesis of scaling data. *Self-similar network traffic and performance evaluation*, 39–88 (2000)
- [79] Veitch, D., Abry, P.: A wavelet-based joint estimator of the parameters of long-range dependence. *IEEE Transactions on Information Theory* **45**(3), 878–897 (1999)
- [80] Azadbakhsh, M., Jankowski, H., Gao, X.: Computing confidence intervals for log-concave densities. *Computational Statistics & Data Analysis* **75**, 248–264 (2014)
- [81] Jaffard, S., Melot, C., Leonarduzzi, R., Wendt, H., Roux, S.G., Torres, M.E., Abry, P.: p-exponent and p-leaders, Part I: Negative pointwise regularity. *Physica A* **448**, 300–318 (2016)
- [82] Mills, J.: Table of the ratio: area to bounding ordinate, for any portion of normal curve. *Biometrika* **18**(3/4), 395–400 (1926)